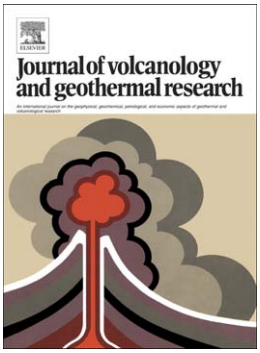

Geological and geotechnical characterization of the debris avalanche and pyroclastic deposits of Cotopaxi Volcano (Ecuador). A contribute to instability-related hazard studies

L. Vezzoli, T. Apuani, C. Corazzato, A. Uttini

PII: S0377-0273(16)30253-0
DOI: doi:10.1016/j.jvolgeores.2017.01.004
Reference: VOLGEO 5983

To appear in: *Journal of Volcanology and Geothermal Research*

Received date: 12 August 2016
Revised date: 19 December 2016
Accepted date: 2 January 2017

Please cite this article as: Vezzoli, L., Apuani, T., Corazzato, C., Uttini, A., Geological and geotechnical characterization of the debris avalanche and pyroclastic deposits of Cotopaxi Volcano (Ecuador). A contribute to instability-related hazard studies, *Journal of Volcanology and Geothermal Research* (2017), doi:10.1016/j.jvolgeores.2017.01.004

Geological and geotechnical characterization of the debris avalanche and pyroclastic deposits of Cotopaxi Volcano (Ecuador). A contribute to instability-related hazard studies

Vezzoli L.[1], Apuani T.[2], Corazzato C.[1], Uttini A.[1]

[1] Dipartimento di Scienza e Alta Tecnologia, Università degli Studi dell'Insubria, Como, Italy.

[2] Dipartimento di Scienze della Terra "A. Desio", Università degli Studi di Milano, Milan, Italy.

Abstract

The huge volcanic debris avalanche occurred at 4.5 ka is a major event in the evolution of the Cotopaxi volcano, Ecuador. The present volcanic hazard in the Cotopaxi region is related to lahars generated by volcanic eruptions and concurrent ice melting. This paper presents the geological and geotechnical field and laboratory characterization of the 4.5 ka Cotopaxi debris avalanche deposit and of the younger unconsolidated pyroclastic deposits, representing the probable source of future shallow landslides. The debris avalanche formed a deposit with a well-developed hummocky topography, and climbed a difference in height of about 260 m along the slopes of the adjacent Sincholagua volcano. The debris avalanche deposit includes four lithofacies (megablock, block, mixed, and sheared facies) that represent different flow regimes and degrees of substratum involvement. The facies distribution suggests that, in the proximal area, the debris avalanche slid predominantly confined to the valleys along the N and NE flank of the volcanic cone, emplacing a stack of megablocks. When the flow reached the break in slope at the base of the edifice, it became unconfined and spread laterally over most of the area of the Rio Pita valley. A dynamic block

fragmentation and dilation occurred during the debris avalanche transport, emplacing the block facies. The incorporation of the older Chalupas Ignimbrite is responsible for the mixed facies and the sheared facies. Geotechnical results include a full-range grain size characterization, which enabled to make broader considerations on possible variability among the sampled facies. Consolidated drained triaxial compression tests, carried out on the fine fraction less than 4.76 mm, point out that shear strength for cohesionless sandy materials is only due to effective friction angle, and show a quite homogeneous behaviour over the set of tested samples.

The investigated post-4.5 pyroclastic deposits constitute a 5-12 m thick sequence of poorly consolidated materials that are interlayered with lava flows. Their geotechnical analyses have evidenced a strong variability in grain size distribution, reflecting the depositional processes, and a generally high porosity. Consolidated drained triaxial compression tests delineated a similar shear stress-strain behaviour among the different units, where shear strength is only due to friction angle. Failure surfaces are always well developed, indicating that the poorly consolidated pyroclastic cover could undergo failure leading to the formation of a gravity driven instability phenomena, like granular or debris flows, which are mainly controlled by the fine fraction.

This work underlies the general necessity for a site-specific, and interdisciplinary approach in the characterization of volcanic successions to provide reliable data for gravitational instability studies.

Keywords

Cotopaxi; debris avalanche; volcano collapse; geotechnical characterization; volcaniclastics grain size distribution.

1. Introduction

The sector collapse of a volcanic edifice and related debris avalanche and lahar flows represent a catastrophic typology of volcanic hazard that affects several stratocones in densely populated regions (van Wyk de Vries and Davies, 2015, and references therein). These events are frequently associated with explosive activity producing great amount of loose pyroclastic materials, or involve poorly consolidated pyroclastic and volcaniclastic deposits mantling the volcano flanks (Lipman and Mullineaux, 1981; Belousov, 1995).

A useful tool to understand the occurrence of volcanic debris avalanches and lahars, their triggering, transport, and emplacement mechanisms is the modelling analysis, either numerical (e.g.; Hürlimann et al 2001; Kelfoun and Druitt, 2005; Patra et al., 2005; Apuani et al., 2007; Thompson et al., 2009; Sosio et al., 2012) or analogue (e.g.; Tibaldi et al., 2006; Shea and van Wyk de Vries, 2008; Andrade and van Wyk de Vries, 2010; Longchamp et al., 2015). These models mainly use as input parameters unit weight, porosity, cohesion, friction angle and viscosity, that are rarely directly determined from in situ and laboratory tests, but more often taken from the literature, including handbooks on general rock and soil properties (i.e., Afrouz, 1992; Bell, 2000) and large-range built-in database included in modelling codes packages.

Despite a crucial aspect of the model validation is the appropriate knowledge and application of the physical parameters of the natural geological bodies involved in the phenomena, and their geological representativeness, they still represent a major source of uncertainty. Actually, at present, in the international literature, few quantitative data exist on direct physical and geotechnical measurements of volcanic material as pyroclastic and volcaniclastic deposits (e.g; Apuani et al., 2005a,b; del

Potro and Hürlimann, 2008, and references therein; Morelli et al., 2010; Schaefer et al., 2013, 2015). Moreover, considering the peculiarities of volcanic environment and volcanic products, and the diversity of materials that compose the edifices, specific geotechnical characterizations should be performed for each single case.

The Cotopaxi volcano (0°40'0"S, 78°26'0"W; Ecuador) is one of the highest (5897 m asl, above sea level) active stratovolcanoes in the world (Fig. 1). It is located along the eastern border of the NNE-trending extensional basin, named Interandean Valley, that separates the Western Cordillera and Eastern Cordillera (or Cordillera Real) of the Ecuadorian Andes (Fig. 1a; Fiorini and Tibaldi, 2012). This narrow structural depression is highly populated, hosting the large urban settlements of Quito (60 km N of the volcano; >1,500,000 inhabitants), Latacunga (45 km S; 120,000 inhabitants), and Ambato (70 km S; 250,000 inhabitants). North of Cotopaxi are the Quaternary extinct Ruminahui and Sincholagua volcanoes; to the SE is the Chalupas caldera (Fig. 1). A summit permanent glacier, about 14 km^2 in extent, 30-70 m in thickness, and ~0.7 km^3 in volume (Jordan, 1983; Cáceres, 2005), caps the present Cotopaxi cone.

At 4.5 ka ago, Cotopaxi experienced a major lateral collapse of the north and northeast flanks forming a debris avalanche (Fig. 1b; Smyth and Clapperton, 1986; Barberi et al., 1995; Hall and Mothes, 2008a) that transformed in the gigantic Chillos Valley Lahar travelling down to the Pacific Ocean, 326 km away (Mothes et al., 1998). During the last twelve centuries, the Cotopaxi volcanic eruptions produced summit glacier melting and generated large lahars, which resulted in major destructive devastations to the settlements around the volcano (Hall and von Hillebrandt, 1988; Barberi et al., 1992; Mothes et al., 2004; Pistolesi et al., 2013). For this reason, the major volcanic hazard in the Cotopaxi region is the lahar hazard generated by volcanic eruptions and

concurrent ice melting (Mothes, 1992; Aguilera et al., 2004; Pistolesi et al., 2014). The potential destructiveness and inundation areas of Cotopaxi lahars were recently modelled (Barberi et al., 1992; Aguilera et al., 2004; Pistolesi et al., 2014). A particular attention was reserved to the last major eruptive and lahar-generating event of AD 1877 (Miller et al., 1978; Hall and von Hillebrandt, 1988; Mothes et al., 2004; Mothes, 2006).

The principal goals of our study are: (a) to contribute the geological, stratigraphical, and sedimentological characterization of the debris avalanche deposit resulting from the 4.5 ka Cotopaxi catastrophic failure; and (b) to quantitatively determine some geotechnical parameters of both the debris avalanche deposit and the recent pyroclastic deposits constituting the poorly consolidated cover of the northern volcano flank.

The usefulness of our study is justified by the need for a quantitative characterization of: (a) the deposit resulting from a debris avalanche process, and (b) the volcaniclastic cover representing both the analogue source of past shallow instability events and a potentially unstable mass that could be easily involved in landslide and lahar phenomena during future eruptions and summit glacier melting.

2. Geological background

2.1 The Cotopaxi volcanic history

The volcanic history of Cotopaxi can be divided in three phases. During the first phase, at about 560-420 ka (fission-track ages; Bigazzi et al., 1997), an ancient stratovolcano, named Cotopaxi I, emplaced rhyolitic domes and caldera-forming pyroclastic deposits in the southern part of the present cone (Fig. 1b; Barrancas rhyolite series in Hall and

Mothes, 2008a). Afterward, a long period of quiescence and erosion took place; it was punctuated by the andesitic lava flows of the Morurcu satellite vent and the deposition of the Chalupas Ignimbrite, sourced from the Chalupas caldera at 211 ka ($^{40}Ar/^{39}Ar$ age of 211±14 ka, Hammersley, 2003).

The second phase of activity (Cotopaxi II; Barberi et al., 1995; Hall and Mothes, 2008a) resumed about 13 ka ago (uncalibrated radiocarbon dates on peat at 13,200±60 a BP from Smyth, 1991, and 13,550±20 a BP from Hall and Mothes, 2008a) with rhyolitic explosive and andesitic effusive eruptions (F rhyolite series in Hall and Mothes, 2008a). This phase culminated at 4.5 ka with rhyolitic domes explosions (Colorado Canyon rhyolite episode in Hall and Mothes, 2008a) and a major lateral collapse of the north and northeast flanks forming a debris avalanche (Fig. 1b; Smyth and Clapperton, 1986; Barberi et al., 1995; Mothes et al., 1998; Hall and Mothes, 2008a).

After the collapse, a new phase of activity was characterized by several andesitic explosive and effusive eruptions and minor rhyolitic events producing the present Cotopaxi cone (Barberi et al., 1995; Hall and Mothes, 2008a; Pistolesi et al., 2011). The first described historical eruption occurred in 1534, at the beginning of the Spanish domination. The last documented major eruption occurred in 1877 (Wolf, 1904), whereas poorly verified eruptions were reported in 1878-1885, 1903-1904, and 1942 (Barberi et al., 1995; Pistolesi et al., 2011). Unrest events occurred in 2001-2002 (Molina et al., 2008; Hickey et al., 2015) and 2015 (http://www.igepn.edu.ec/informes-volcanicos/cotopaxi).

2.2 The 4.5 ka lateral collapse of the Cotopaxi volcano

The Cotopaxi debris avalanche (DA) deposit involved the northern and northeast foothill of the volcano, having run downslope for 25 km in the upper part of the Rio Pita valley, and ramped on the slopes of surrounding volcanoes for several hundred of metres (Fig. 2). The estimated covered area is 138 km^2 (Hall and Mothes, 2008a) and the proposed original volume is about 2 km^3 (Mothes et al., 1998; Hall and Mothes, 2008a). The collapse scar is not clearly discernible because of the filling by products of the subsequent volcanic activity. The surface morphology of the DA deposit is a typical well-preserved hummocky topography. The hummocks relieves are capped by a continuous cover of recent pyroclastic fall layers interbedded with paleosols (Barberi et al., 1995).

The DA deposit is described as a tuff-breccia composed of angular clasts of obsidian, banded rhyolites, grey aphyric rhyolites, andesite, dacite and rhyolite lavas, in a coarse ash matrix of the same lithologies (Barberi et al., 1995; Mothes et al., 1998; Hall and Mothes, 2008a).

The DA is associated with a debris flow (Chillos Valley Lahar, CVL; Mothes et al., 1998). The CVL deposit is a single, homogeneous, and beige-tan coloured flow unit in either the proximal or distal outcrops. It mainly consist of a predominant pumice-rich ashy matrix and scattered lithic clasts. The matrix material is interpreted as fresh, juvenile pyroclastic products of rhyolitic composition. The total CVL wet volume is estimated of 3.8 km^3 (Mothes et al., 1998).

The ^{14}C age of the DA formation was firstly determined at about 5000 a BP (uncalibrated 3460±140, 4170±110, and 5010±210 a BP) by Barberi et al. (1995) on paleosols interbedded within the pyroclastic sequence overlying the DA hummocks. The age of the event was subsequently refined at 4600-4500 a BP on the basis of ^{14}C

dating on paleosols beneath the Colorado Canyon pyroclastic ash flows deposits (uncalibrated 4420±80 and 4670±70 a BP; Smyth, 1991), and of archaeological finds covered by the CVL deposit (Mothes et al., 1998).

The presence of an explosive activity accompanying the lateral collapse is questioned. Objectively, pumiceous pyroclastic material occurs associated with the DA and CVL deposits or is locally compenetrated with the lithic components.

Smyth and Clapperton (1986) suggested that the emplacement of the debris avalanche was associated with an explosive eruption and the emplacement of a pyroclastic flow.

Barberi et al. (1995) interpreted that older unconsolidated pyroclastic deposits mantling the cone flanks were mixed downstream during the flow of the debris avalanche.

Mothes et al. (1998) and Hall and Mothes (2008a) considered that the collapse was intimately associated with several rhyolitic explosive events named “Colorado Canyon rhyolite episode”. These authors proposed a sequence of events comprising: (a) the phreatomagmatic explosion and collapse of older domes of the F Series with the emplacement of thin obsidian-rich sand/pumice lapilli layers and a rhyolite breccia flow; (b) a major plinian explosion with the emplacement of pumice lapilli fall and ash flow deposits (Colorado Canyon Pyroclastic Flow-I, CCPF-I) with mineralogical and geochemical composition identical to the Chalupas ignimbrite; (c) the sector collapse of the north-eastern flank of Cotopaxi's cone (composed of an andesitic stratocone and rhyolitic domes) forming the debris avalanche deposit; (d) a second minor emplacement of ash flows (CCPF-II) that melted the fractured icecap, became saturated with water, and immediately and almost entirely transformed into the CVL near the base of the cone; and (e) the final ash flow eruption (CCPF-III) that overlies both CCPF-II and CVL.

Moreover, at many outcrops, chaotic or inverted stratigraphic relations exist among the different lithologies, suggesting that many events are contemporaneous or closely related in time.

2.3 The recent (post-collapse) eruptive activity of the Cotopaxi volcano

The stratigraphy and geochronology of the succession of tephra layers interbedded with paleosols representing the Cotopaxi explosive activity during the last 4.5 ka were described by Barberi et al. (1995). These Authors recorded the products of 20 plinian (VEI 3–4) andesitic explosive eruptions in the last 2000 years, and recognized at least 10 other pyroclastic layers in the sequence comprised between this age and the DA deposit (Fig. 3a).

Pistolesi et al. (2011) identified 21 main tephra beds during the past eight centuries, from the AD 1140 Quilotoa ash (emitted from the Quilotoa caldera; Fig. 1a; Hall and Mothes, 2008b; Di Muro et al., 2008) to the last large eruptive event of Cotopaxi occurred in 1877 (Fig. 3a). The detailed eruptive chronology of these tephra beds were subdivided in three eruptive periods (Pistolesi et al., 2011). The first eruptive period (AD 1150 to 1534) was characterized by two mid-intensity explosive eruptions (tephra layers B_L and S_W in Fig. 3a). Activity of the second period coincided with two plinian eruptions in 1742–44 (tephra layer M_T) and 1766–68 (tephra layer M_B) that were associated with the formation of scoria flows (layer $M_{S;}$ Fig. 3a). The third period was characterized by a quasi-persistent activity, mainly represented by a moderate-intensity ash emission with episodic low-magnitude sub-plinian eruptions and boiling-over effusions, which generated scoria flow deposits (tephra layers M_V, P_D, P_L, P_E, and P_R in Fig. 3a). Pistolesi et al. (2013) integrated the chronostratigraphy of the

recognized tephra beds with the lahar deposits sequence cropping out around the volcano in a comprehensive stratigraphic reconstruction, which allowed to correlate the debris flow events to their generating explosive eruptions.

3. State of the art on the physical and mechanical characterization of volcaniclastic materials

3.1 Overview on volcanic material characterization

The physical, geotechnical and geomechanical characterization of volcanic materials (including soils, rocks, and rock masses) has revealed to be a major challenge since numerical analyses have begun to quantitatively approach landslide phenomena (lateral collapses, debris avalanches, debris flows) in volcanic environments after the Mt. St. Helens' 1980 event.

In recent years, the International Association of Rock Mechanics (ISRM) has shown increased interest in volcanic materials, and has dedicated specialised conferences on rock mechanics and geo-engineering in volcanic environments. These produced thematic volumes (Dinis da Gama and Ribeiro e Sousa, 2002; Malheiro and Nunes, 2007; Olalla et al., 2010; Rotonda et al., 2016), collecting case-histories and solutions proposed. As for most geotechnical studies, these case histories refer to local engineering projects and consider local-scale investigations in homogeneous rock masses; only very few are related to hazard and risk assessment associated to large slope instability in active volcanic areas. Studies on the physical and mechanical characterization of volcanic materials have been mostly focused on massive and strong rock masses as lavas and alternating lava and autoclastic breccia successions (e.g. Watters et al., 2000; Okubo, 2004; Thomas et al., 2004; Apuani et al., 2005a;

Moon et al., 2005; Schaefer et al., 2015). del Potro and Hürlimann (2008) are the first to suggest a unifying geotechnical classification of volcanic materials encompassing all geotechnical units potentially found in volcanic areas, combining their new data with an extensive literature review.

In volcanic environments, the application of standard engineering classifications and procedures has to comply with:

i) The intrinsic and diverse nature of volcanic products (rock masses - massive to highly fractured, weak rocks, loose deposits). According to del Potro and Hürlimann (2008), massive lavas and pyroclastic rocks can be investigated, classified and parametrised as strong rock masses, with variable degree of fracturing. On the contrary, loose pyroclastic deposits, debris avalanche deposits and lahar deposits can be parametrised with the standard geotechnical methodologies for soils ("soil" in an engineering geological sense; Smith, 1982). Other materials, instead, constitute rock masses that cannot be classified as either strong rock masses or soils, but are borderline and constitute the category of the "weak and complex rock masses" (Esu, 1977; Oliveira, 1993; Evangelista and Picarelli, 1998): these are the most difficult materials to be approached and characterised.

ii) The unknown interior structures and geometry of the edifice and the geological complexity (heterogeneity, anisotropy, outcrop continuity, representative volumes) originated from the emplacement mechanism. The most relevant geological complexity is shown by debris avalanche and lahar deposits, which have an extreme variability in grain size distribution, and a complex spatial distribution. Representative sample volumes are large and generally exceed the sampling limit, and it is very difficult or impossible to preserve the in situ structure.

iii) The often-inaccessible locations of outcrops and related logistical problems, especially on active volcanoes.

Overall, these difficulties discourage from direct field measurements and laboratory testing the volcanic materials, and a large number of modelling studies devoted to volcanic hazard assessment rely only on the generic use of available published data, often related to completely different volcanic materials and conditions, instead of site-specific information. This procedure can generate large uncertainties in the modelling results and could be inadequate to represent the case under study.

In the following overview, we considered only the volcaniclastic materials, because the focus of our geological field and experimental work are the pyroclastic and debris avalanche deposits of the Cotopaxi volcano.

3.2 Pyroclastic deposits and rocks

del Potro and Hürlimann (2008) geotechnically distinguished “strongly welded” (fresh or altered) and “weakly welded and/or interlocked” pyroclastic rocks. Loose pyroclastic deposits are ascribed to the very broad “volcanic soil” unit, gathering all materials with a granular behaviour (cohesive and cohesionless), regardless their origin. This is the weakest unit within volcanic edifices and the most significant in controlling the development of slope instabilities such as debris flow, slide, slump, and avalanche.

The physical characteristics of pyroclastic rocks and deposits (i.e.; grain size distribution, vesicularity, porosity, textural features) were broadly analysed and sufficiently well-know from volcanological works devoted to the study of explosive eruptions’ mechanisms.

“Strongly welded” pyroclastic rocks are generally treated as fair quality fractured rock masses as done for lava successions, for which the Rock Mass Rating (RMR; Bieniawski, 1989), but more often the Geological Strength Index (GSI; Hoek et al. 2001; Hoek et al., 2002; Marinos et al, 2007), are applied to obtain rock mass quality and strength parameters.

Geotechnical strength properties (uniaxial compressive strength - UCS, Young’s modulus, and tensile strength) of “weakly welded and/or interlocked” pyroclastic rocks are obtained applying field and laboratory measurements (Schmidt hammer’s, point load, uniaxial compressive test) carried out on the different parts of the sample (i.e., matrices, clasts or cores) (Moon, 1993; Watters et al., 2000; Ludovico Marques and Delgado Rodrigues, 2002; Crosta et al., 2005; del Potro and Hürlimann, 2008; Gonzalez de Vallejo et al., 2008).

Published geotechnical data for “volcanic soils” (mostly cohesionless materials) obtained by different authors (Voight et al., 1983; Franz and Voight, 1995; Watters et al., 2000; Hürlimann et al., 2001; Rolo et al., 2004; Apuani et al., 2005a,b; Crosta et al., 2005; Moon et al., 2005; del Potro and Hürlimann, 2008; Gonzalez de Vallejo et al., 2008) include: (a) total and dry unit weight; (b) porosity; (c) shear strength parameters (peak and residual cohesion and friction angle); and (d) tensile strength. In a few cases data were validated by back analyses of known failed slopes.

3.3 Volcanic debris avalanche deposits

Despite a large number of works have been published on volcanic debris avalanche deposits around the world since Mt. St. Helens’ event (van Wyk de Vries and Davies, 2015, and references therein), they usually deal with accurate geological,

sedimentological, textural, and morphological descriptions of the deposits, but only very few studies attempted a characterisation from a geotechnical point of view.

Most of them were devoted to obtaining physical properties of some or all their facies by density measurements and grain size analyses (Voight et al., 1983 and Glicken, 1996 at Mt. St. Helens; Belousov et al., 1999 at Shiveluch; Cortez et al., 2010 at Colima; Moon et al., 2005 at White Island; Morelli et al. 2010 at Tancitaro; Roverato et al., 2015 at Taranaki), and Atterberg limits (Morelli et al. 2010). Those results were mainly used to investigate processes of disaggregation and comminution during DA transportation after failure has occurred. Morelli et al. (2010) also reconstruct the rheological behaviour (yield shear strength, bulk friction angle, viscosity, friction coefficient, turbulence coefficient) by modelling. Few other authors also provided shear strength parameters, namely cohesion and friction angle, and earth pressure coefficients by direct laboratory tests (Voight et al., 1983; Morelli et al., 2010) or by back analyses on historical landslide events (Moon et al., 2005; Morelli et al. 2010).

4. Materials and Methods

4.1 Field geological survey, terminology, and sampling

The original fieldwork included a geological, lithostratigraphic, geomorphological, and structural survey. In particular, we accurately mapped the areal distribution of the DA deposit, with the support of aerial photographs (1:60,000 scale, 1993, Instituto Geografico Militar, Quito, Ecuador, Projecto Carta Nacional) and topographic maps (1:25,000, year 1979, and 1:50,000 scale, 1989, Instituto Geografico Militar, Quito Ecuador). We focused only on the DA deposit exposed at the foothill of the northern sector of the volcano. Furthermore, we described the DA stratigraphic and geometric

relations with both the associated rocks of the Colorado Canyon rhyolite episode (Hall and Mothes, 2008a) and older units, based on over 45 measured sections (Fig. 2). The DA internal sedimentary architecture is mainly exposed in the river scarps of the Rio Pita gully, along the aqueduct way, and in few eroded hummocks. In Fig. 2, only the stratigraphic sections that were sampled for the physical and mechanical analyses are numbered. The detailed analysis of the composition, textures, and internal structures of the DA deposit allow identifying several lithofacies. In the DA facies identification and description, we have taken into account the suggestions of Crandell et al. (1984), Glicken (1991; 1996), Ui and Glicken (1986), Ui et al. (1986), Palmer et al. (1991), Schneider and Fisher (1998), Mehl and Schmincke (1999), and van Wyk de Vries and Davies (2015). We have applied the term “matrix” as its original meaning in sedimentology (Jackson and Bates, 1997) that refers to the relative size of particles (ensemble of smaller particles that englobes coarser particles) and does not imply a predefined particle size fraction (in particular, it is not referred exclusively to particles with grainsize <2 mm). Moreover, we have defined as inter-clast matrix all the material surrounding the DA megablocks and blocks, and as intra-clast matrix the material within a shattered DA megablock or block.

The simplified distinction between “block” facies and “matrix” facies was proposed firstly by Glicken (1991; 1996) as terms useful to define mappable areas of a DA deposit. This nomenclature was further applied at several DA deposits in the literature, but with different meanings. We have adopted the facies nomenclature of DA deposits proposed by Mehl and Schmincke (1999) that is based on: (a) the dimension of blocks, separated in megablocks (>100 m) and blocks (<100 m); (b) the origin of blocks in “primary”, derived from the source volcano, and “secondary”, eroded from the ground

surface during transportation of the avalanche; and (c) the degree and type of deformation of the deposit.

Description and sampling of 8 different sites were carried out, between 3712 and 4555 m asl (Fig. 2; Tab. 1). Four samples of the DA deposit related to the 4.5 ka failure event and four samples of the poorly consolidated recent pyroclastic deposits mantling the Cotopaxi northern flank have been collected. Sampled lithologies were chosen because representative of lithotechnical units involved in the slope instability. Lithotechnical units are an engineering geological type of unit characterized by coupling lithology with physical and mechanical properties. Sampling was carried out along natural outcrops or with manual excavation at <1 m depth. Consequently, samples are disturbed, representative of the nature of materials but not of their structure. Based on the grainsize, sample weight ranges between 16.5 kg for coarser and 4.5 kg for finer materials (Tab. 1).

DA deposit samples (5-12, 4-12, 6-12, and 7-14) have been chosen along a transect in the main direction of the debris avalanche flow path at 7.6 km, 7.8 km, 8.7 km, and 12 km from the present summit crater, respectively (Fig. 2). Samples 5-12, 4-12, and 6-12 come from the megablock and block facies (Figs. 2 and 4), while sample 7-14 belongs to the mixed facies (Fig. 4). The DA samples represent the fraction of the deposit less than 128 mm in size.

Pyroclastic deposit samples (1-11, 2-11, 3-11, and 8-14) have been chosen along the stratigraphic sequence mantling the volcano northern flank (Figs. 2 and 3b) and represent the most significant lithologies of the outcropping pyroclastic deposits (Fig. 4). All the sampling sites of the pyroclastic cover are at the interior of the proximal hazard zone boundary (PHZB), defined as the line that separates erosive from

accumulative areas of lahars (onset of deposition) (Iverson et al., 1998; Pistolesi et al., 2014).

4.2 Physical and mechanical analysis

In the present work, the studied volcaniclastic materials were considered and analysed as “soils” in an engineering geological sense (Smith, 1982), which means cohesive or cohesionless loose granular materials, regardless their composition and origin. The measured geotechnical properties regard: particle size distribution, unit weight at minimum (e_{min}) and maximum (e_{max}) void index ratio, natural water content, and shear strength properties (Tab. 2). Due to the wide range in grain size, some in situ analyses were necessary to properly define the material features, at the outcrop scale. Figure 5a shows the representativeness of the measured tests with the comparison between the grain size fraction sampled and submitted to the tests and the bulk grainsize distribution of the DA and pyroclastic deposits. Type and application of the performed in-situ and laboratory tests are resumed in Table 2, with the standard reference used (ASTM, American Society for Testing and Materials; see the Appendix), when possible. The laboratory analyses were carried out in the Engineering Geology Laboratory for Material Testing of the Earth Science Department of the University of Milan.

Grain size analyses of volcaniclastic materials are usually performed only in the USCS classification range (the portion less than 75 mm; Fig. 5a), while we retained it was important to characterise also the coarser material (up to 256 mm in size; Fig. 5a), to make broader considerations on possible variability among the sampled facies and provide more complete insights on the origin of the deposits. Grain-size distributions were thus determined by combining data (Fig. 5) from: (a) image analysis on field

photographs by measuring the particle size (medium axis) at each node of a 10-cm-spaced grid overlapping a 1 m^2 vertical and smooth exposure (Fig. 5b; grain size > 128 mm; Kellerhals and Bray, 1971; Adams, 1979), (b) in situ calliper (128, 64, 32, and 16 mm) and sieve (8 mm) analyses, and mass determination by mechanical steelyard (grain-size between 128 and 8 mm; Fig. 5c), (c) standard laboratory sieve analysis (grain-size between 8 and 0.074 mm; Fig. 5a), and (d) hydrometer (sedimentation) analysis (grain-size <0.074 mm; Fig. 5a). Grain size fields were based on the ASTM standard (Fig. 5a).

In-situ natural unit weight (γ_n) and angle of repose (φ) were determined in the field for all the collected samples (Tab. 1), before performing the sieving analysis. The non-standard procedure for in-situ unit weight measurements consisted in excavating a cavity at the sampling site, determining the mass of the whole sampled material, and measuring the volume of the irregular hole by water infilling after the positioning of an insulating plastic sheet, as in Apuani et al. (2005a). Also the angle of repose was measured on the total removed material. Sorting and average particle diameter (d_m) were determined on the grain size <128 mm applying the sedimentological methods of Folk and Ward (1957).

High resolution X-ray powder diffractometry was also performed on the fine fraction (<0.074 mm; > 12%; Fig. 5a) of sample 3-11, to identify its mineral composition.

Consolidated-drained triaxial compression tests (ASTM D7181) were carried out on reconstituted specimens at a chosen unit weight (γ_d in Tab. 4) close to its maximum value (γ_{max} from e_{min}; Tab. 3). It was decided to use only the fraction minor than 4.76 mm to form specimens of 70 mm in diameter (Fig. 5a), so as to minimize the possibility of rupture of the rubber membrane due to the high asperity of coarser clasts. Since it is

not possible in the geological and geotechnical context to sample undisturbed granular samples, the use of reconstructed specimens in granular soil is common and recommended, provided that the standard procedures of reconstruction (ASTM D7181) are strictly followed. Furthermore, this is necessary to obtain results comparable to data provided in literature. The tests were carried out in the range 32-180 kPa of minor principal effective stress (σ_3'), justified by the 5-10 m thickness of the deposits that could be involved in shallow mobilization.

5. Results on volcano geology and geotechnical properties

5.1 The 4.5 ka Debris Avalanche deposit

5.1.1 Morphology and distribution

The studied proximal part of the DA deposit occupies the broad depression drained by the Rio Pita, between the northern and north-eastern basal flanks of the Cotopaxi cone and the south-western flank of Sincholagua volcano (Figs. 1b and 2). The Cotopaxi DA deposit shows a well-developed hummocky surface morphology (Figs. 6a, b; Glicken, 1991) with a relatively undissected surface. The height of the mounds above the present topographic surface diminishes with distance from the source (Crandell et al., 1984; Yoshida, 2013). The maximum elevation of hummocks is 215 m above the adjacent flat area to the north. Approximate relief of hummocks above Rio Pita flood plain is <10 m.

The topographic expression of the hummocks is reduced by subsequent tephra cover and historical scoria and debris flow burial (Fig. 6c; Barberi et al., 1995). These overlying units maintain their thickness across the hummock's surface in proximal outcrops where they are only pyroclastic fall deposits (Fig. 6c), whereas they thicken in

swales between the hummocks and thin over the tops, where debris flow deposits are intercalated to smooth the topographic surface.

Distribution of facies suggests that the debris avalanche flowed predominantly confined to the valleys W and E of the Ingaloma hill (Fig.s 1 and 2) as far as it reached the break in slope at the base of the edifice, where the flow became unconfined and spread laterally over most of the area of the Rio Pita valley.

Today, the most proximal DA outcrops are found at about 8 km from the cone summit, at Ingapirga and Ventanillas exposures, that are located at an elevation of 3960 m asl to the NW and 3880 m asl to the NE of Ingaloma hill, respectively (Fig. 2). The northern lowest occurrence of the DA deposit that we have mapped is at 3670 m asl along the Rio Pita valley near the Gate North of the Cotopaxi National Park (Fig. 2). The north-western boundary of the DA deposit is along the E slope of the Ruminahui volcano at 3980 m asl. Towards the NE and E, the DA deposit climbed the slopes of Sincholagua volcano up to an elevation of 4000-4020 m asl and moved along the floor of its radial valleys for about 1.5 km (Fig. 2). The easternmost boundary is in the El Mudadero locality, where the DA deposit is in the Rio Carcelen up to 4030 m asl and in the Chorro de Pansaloma up to 4045 m asl (Fig. 2). The maximum DA runout distance before the transformation in a debris flow is reconstructed to be about 20 km to the N (from the Yanasacha scarp at 5500 m asl to the distal front at 3670 m asl), for a drop height of 1830 m (Fig. 2). The DA run-up the Sincholagua flank along the Quebrada Tungurahua for about 32 km, reaching the elevation of 4040 m asl (Fig. 2). Because the base of the DA deposit is rarely exposed, determination of its thickness and volume is strongly speculative.

5.1.2 Stratigraphy

The basal contact of the Cotopaxi DA deposit is rarely exposed. Stratigraphically, the DA deposit overlies the Chalupas Ignimbrite along the southern slopes of Sincholagua volcano and the Rio Pita valley. The base of the deposit is exposed only in the distal eastern outcrops in the streambed of the Rio Carcelen (Fig. 6d). At this locality, the contact appears to be planar and sharp, without erosional or scouring structures. The Chalupas Ignimbrite is composed of a whitish lapilli tuff comprising an abundant ashy matrix and dispersed pumice clasts. Pumices are white in colour, poorly vesiculated to dense, 1-2 cm in maximum size.

The top of the DA deposit is observable over a widespread area. A plane-parallel stratified succession of tephra layers interbedded with paleosols, representing the Cotopaxi explosive activity during the last 4.5 ka (Barberi et al., 1995; Pistolesi et al., 2011), overlies the DA deposit with a thickness up to 5 m (Figs. 6b, c). Locally, in the proximal outcrops, the DA deposit is sharply overlaid by a pyroclastic flow deposit, composed of prevailing ash and sparse pumice clasts, that can be correlated with the Colorado Canyon pumice flow unit III of Hall and Mothes (2008a). In the distal outcrops, the upper contact of the DA block facies is transitional to a matrix-supported, pumice-rich breccia with subordinate lithic fragments, that can be correlated with the Chillos Valley lahar unit (Fig. 2) of Mothes et al. (1998) and Hall and Mothes (2008a).

5.1.3 Lithology and Sedimentology

Overall, the DA deposit is composed of a lithic megabreccia, massive and poorly sorted, from medium to well consolidated, with a variable grainsize, texture, and amount of coarse matrix. Based on size and composition of clasts and texture of the

DA deposit, we distinguished four lithofacies (Mehl and Schmincke, 1999): 1) megablock facies; 2) avalanche block facies; 3) mixed facies; and 4) sheared facies. These facies undergo lateral transitions and complex sedimentary architecture.

Megablock facies

The megablock facies was mainly deposited in the proximity of the volcano and is exposed in the NE slope between Ingaloma, Ventanillas and the Rio Pita (Fig. 2), where it forms a cluster of hummocks, each composed of a megablock with single lithology. The distance from the present volcano summit is 9.7-7.8 km. This facies is characterized by megablocks, several decametres large (max 215 m high and 400 m in length; Fig. 6b) that represent intact portions of the edifice-derived pre-failure lavas, slightly disaggregated and deformed (toreva blocks). Even though most of the blocks are fractured or shattered, they retain a recognizable geometry and original bedding and layering (Ui and Glicken, 1986; Shea and van Wyk de Vries, 2008) as the primary depositional and cooling structures of lava flows and stratigraphic contacts (Fig. 7a). In the megablocks, the fragmentation degree changes from the core, that is coherent or with close fractures and jigsaw cracks (Figs. 7a, b), to the margin, that is jigsaw-fit fragmented and grades into an external aureole of brecciated blocks with intra-clast matrix (Fig. 7c).

The megablocks are mainly constituted of andesitic and dacitic lavas. Lithological domains are well distinct. Lavas are composed of the following lithologies: (a) andesite, massive, locally scoriaceous, dark grey or tan coloured, poorly porphyritic (porphyricity index, PI, 5-15%) with small (<1 mm) phenocrysts of plagioclase and pyroxene in an aphanitic groundmass (sample 6-12; Fig. 4b); (b) andesite, massive, light brown and

reddish in colour, poorly porphyritic (PI 5-10%) with phenocrysts of plagioclase and pyroxenes up to 4 mm; and (c) dacite, dark grey to black coloured, aphyric (PI <1%), with scarce phenocrysts of amphibole, pyroxene, and plagioclase. The inter-clast matrix is composed of a clast- to matrix-supported breccia, with sub-angular to sub-rounded clasts, 0.02-1 m in size, with the composition of the adjacent megaclasts (Fig. 4a). Hydrothermally altered lavas are locally present (sample 4-12; Fig. 4a).

Block facies

The block facies is the prominent type in the DA deposit, and it is distributed mainly in the middle, distal and marginal areas of deposition (Fig. 2). It also surrounds the megablocks along the Victor Puñuna valley at 3920-3900 m asl. It consists of clasts and a finer-grained matrix (Siebert, 1984; Schuster and Crandell, 1984; Glicken, 1991). The proportion of clasts and matrix is irregular and varies from a clast-supported texture with minimal or no inter-clast matrix (block-against-block architecture; Fig. 7d) to matrix-supported texture. Clasts are composed of angular and heterolithologic blocks ranging from a few decimetres to more than a few tens of metres in diameter. In proximal outcrops, bigger blocks are either fractured or shattered, and many of the block interiors exhibit pervasive jigsaw cracks and jigsaw-fit texture (Figs. 4c and 7e; Ui, 1983; Glicken 1991, 1996). The blocks with jigsaw-fit texture show an intra-clast matrix comprising a clast-supported monogenetic breccia composed of angular clasts with the same composition of the block (Fig. 7e). In the distal area, angular fragments are completely disaggregated and dispersed. Numerous clasts with jigsaw-fit texture have fractures filled with inter-clast matrix material (Glicken, 1996; Mehl and Schminke, 1999).

Rock types present in the block facies include, in addition to the types (a) and (c) of the megablock facies: (d) vitrophyric rhyolite, generally massive, locally vesiculated, light grey to pinkish in colour, with phenocrysts (PI 15-20%) of plagioclase (3-4 mm) and scarce smaller mafic minerals in a glassy groundmass; (e) vitrophyric banded dacite, with phenocrysts (PI 10-15%) of plagioclase (3-4 mm) and biotite; and (f) black obsidian. Hydrothermally altered volcanic rocks are very rare in block facies deposits.

Mixed facies

The mixed facies developed by the mixing of the DA block facies with accidental substratum materials (Friedmann, 1997) picked up by the debris avalanche during transport. The mixed facies is a chaotic assemblage of matrix-supported clasts of: (a) DA blocks and single fragments of fractured and shattered lavas; (b) white pumices, poorly vesiculated to dense, 1-2 cm in maximum size; and (c) pyroclastic rocks, stratified, composed of interbedded layers of ash and lapilli (Fig. 4d). Clasts are angular to rounded. The inter-clast matrix is mainly composed of unsorted and disaggregated ash and pumice lapilli lithologically similar to the clasts. Individual DA blocks within the mixed facies are geometrically distinct, and range in size from 0.1 m to several metres in diameter. The mixed facies developed near the Ingaloma hill and along the Rio Pita valley (Fig. 2), where the DA deposit was laterally in contact with and overlaid on the Chalupas Ignimbrite. On the basis of the lithology and geometrical relationship, we suggest that the pyroclastic component (both clasts and inter-clast matrix) of the mixed facies belongs to the Chalupas ignimbrite as a secondary component, ripped-up during the DA flow.

Sheared facies

Along the banks of the Rio Pita incision, intact to folded and highly brecciated blocks of the Chalupas Ignimbrite, which are tens to several hundreds of metres in size, were found intrinsically compenetrated with the lava and scoria blocks of the DA deposit (Fig. 2). This “mélange” of blocks of different lithotypes has been strongly deformed as a whole by faulting and folding during avalanche emplacement (Fig. 7f).

We retain that the large proportion of Chalupas Ignimbrite included in the DA deposit along the Rio Pita was not related to the involvement of this unit in the volcano landslide but the incorporation of substrate-derived, poorly consolidated pyroclastic rocks in the debris avalanche deposit, as in other collapsed volcanoes (e.g.; Chimborazo; van Wyk de Vries and Davies, 2015).

5.1.4 Geotechnical properties

Grain size analyses were performed on all the four samples of the DA deposit, namely 4-12, 5-12, and 6-12 from the proximal zone, and 7-14 from the distal zone (Tab. 1 and Fig. 2). The total grain-size distribution (Fig. 8a and Tab. 3, all soil fractions) of the DA samples shows the greatest variability (up to 28%) in the size range from coarse sand to boulders, while there are no significant differences in the amount of the fine fraction (<0.074 mm): the cumulated silt and clay content is very low, ranging from 5 to 9%, always with a negligible clay fraction (<0.01%).

Based on laboratory tests performed on the portion of soil samples passing the 75 mm sieve (Fig. 5a and Tab. 3, soil portion < 75 mm), namely grain size, coefficient of uniformity (Cu) and coefficient of curvature (Cc), the analysed DA deposits can be classified according to the Unified Soil Classification System (USCS; ASTM D2487) as

SP-SM (poorly graded sand with gravel and silt) or GP-GM (poorly graded gravel with sand and silt; sample 6-12) (Tab. 3). Dual symbols are required being fines between 5 and 12%. The sorting coefficient ranges 3.26-3.87 phi, typical of very poorly sorted sediments.

Minimum and maximum porosity (n) of the dry soil portion less than 8 mm, calculated from maximum and minimum dry unity weight (γ_d) measurements (ASTM D4254), range 6-20% for n_{min} and 16-38% for n_{max} (Tab. 3), which correspond to 11.8 kN/m^3 < γ_d < 18.6 kN/m^3.

Consolidated drained triaxial compression tests (ASTM D7181) were carried out on all the DA samples in the range 32-154 kPa of minor principal effective stress (σ_3'). The deviatoric stress (σ_1' - σ_3'; kPa) and change in volume ($\Delta V/V_c$) versus axial deformation (ε; %) plots are reported as an example (samples 6-12 and 7-14) in Figure 9a, with different applied σ_3'. Shear strength is only due to friction angle, as it is for all cohesionless sandy materials. The shear strength angles at failure (ϕ'_f) are: 47° (sample 4-12), 52° (5-12), 56° (6-12) and 53° (7-14). Failure surfaces are well developed (Fig. 9c, sample 7-14). Shear stress (τ') versus normal stress (σ') graph and Mohr stress circles at failure are reported as an example (sample 4-12) in Figure 10a. s' (centre of the Mohr stress circle - one half the sum of the major and minor effective principal stress) versus t' (radius of the Mohr stress circle - one half the sum of the major and minor effective principal stress) graph, obtained from each sample, and linear regression for shear strength parameter calculation are also presented (Fig. 10b). The residual shear strength parameters (ϕ'_r) are: 40° (sample 4-12), 42° (5-12),

44° (6-12) and 43° (7-14). Overall, the analyzed samples show a quite homogeneous geotechnical behaviour.

5.2 The post 4.5 ka pyroclastic deposits

5.2.1 Stratigraphy and lithology

The investigated pyroclastic deposits constitute a 5-12 m thick sequence of stratified and poorly consolidated pyroclastic materials that are interlayered with the lava flows of the post-4.5 ka activity (Fig. 3; Barberi et al., 1995; Pistolesi et al., 2011). On the northern flank of the Cotopaxi volcano, the Quebrada Yanasacha exemplifies a typical valley along the volcano's flanks, showing a steep (>20°) baseline and a morphology of a narrow canyon laterally confined by vertical stacks of lavas and pyroclastic sequences. The lithological discontinuity between coherent strata (lavas and spatter) and loose pyroclastic deposits (Fig. 11a) represents the most probable detachment surface that could lead to the formation of a gravity-driven instability phenomenon like a granular flow or a debris flow. The pyroclastic sequence is mainly constituted of interlayered ash beds, agglutinated scoriae, pumiceous and scoriaceous lapillistones of fall-out origin, dune–bedded ash deposit of pyroclastic surge origin, and lahar deposits constituted of matrix-supported lithic breccia. Four stratigraphic sections represent the complete stratigraphic sequence of the northern flank (Figs. 2 and 3b) as reconstructed by Barberi et al (1995) and Pistolesi et al. (2011) (Fig. 3a).

In section 1 (Figs. 2 and 3b), the contact between a sequence of lava flows (Yanasacha lava) and the volcaniclastic cover is visible. The pyroclastic unit is a 3 m thick massive, clast-supported, welded coarse breccia composed of scoriaceous lapilli and bombs, from scarce to well sorted (sample 2-11; Figs. 4e and 11c). Scoria are

subrounded, max 40 cm in size, coarse vesiculated. Lithic clasts are rare. The deposit is well consolidated because of agglutination of scoria. Textures suggest a pyroclastic fall genesis from lava fountains.

In section 2 (Figs. 2, 3b and 11b), the pyroclastic sequence is represented by the interbedding of medium to coarse ash and lapilli layers. Ash layers are both well sorted and massive (sample 3-11; pyroclastic fall deposit) and well to medium sorted, wave and cross laminated, with irregular beds of pumice and lithic lapilli, with a maximum thickness of 90 cm (pyroclastic surge deposit). Lapilli layers are well sorted and massive, locally with normal grading, 10-60 cm in thickness, composed of predominant white pumices, black scoriae, and subordinate lithic clasts (sample 8-14). At least four pedogenized horizons are present.

In section 3 (Figs. 2, 3b and 11c), the pyroclastic sequence is interlayered with debris flow deposits and show unconformities and erosive surfaces. Debris flow deposits are massive, normal-graded matrix-supported polygenetic breccia, with a variable thickness ranging from 60 cm to 300 cm.

Section 4 (Figs. 2, 3b and 11d) represents the products of historical eruptions. The deposit is loose, composed of irregular ash and lapilli beds, from few centimetres to decimetres thick, with poorly defined contacts (sample 1-11). Ash is coarse, massive or stratified, locally with sparse lapilli of pumices and lithics, 0.5-5 cm in size. Lapilli beds are medium to poorly sorted, clast-supported, composed of whitish and grey pumices, 4-5 cm in size, and lava lithics.

5.2.2 Geotechnical properties

The same geotechnical analyses performed on DA samples were also carried out for pyroclastic deposits samples. These show a strong variability in grain size distribution (Fig. 8b) and coefficient of uniformity (Cu), from silty sand (fine fraction 23%) to well graded gravel with sand (negligible fine fraction, with 81% of gravel) (Tab. 4).

Sand fraction greatly dominates in the ash sample 3-11 (SM, silty sand) and in the loose reworked scoriaceous and pumiceous sample 1-11 (SP-SM, poorly graded sand with gravel and silt). Gravel fraction dominates in the scoriaceous lapillistone sample 8-14 (GW, well graded gravel with sand) and in the agglutinated scoria sample 2-11 (GP-GM, poorly graded gravel with sand and silt) (USCS; ASTM D2487). The better-sorted samples are 3-11 (phi = 3.1, Cu = 74) and 8-14 (phi = 1.4, Cu = 7; Tab. 4), reflecting their fallout origin despite their very different mean grain value (d_m).

Minimum and maximum porosity (n) of the dry soil portion less than 8 mm are very high, ranging 18-26% for n_{min}, 31-44% for n_{max} (Tab. 4).

Sample 3-11was analysed by X-ray powder diffractometry, which revealed a composition of vermiculite, and subordinate albite, quartz and hornblende.

Consolidated drained triaxial compression tests (ASTM D7181) were carried out on samples 1-11, 2-11 and 3-11, while sample 8-14 was discarded because mainly constituted of gravel with high-asperity clasts. The minor principal effective stress (σ_3') ranges 43-180 kPa. Examples of the results are reported in Figures 9b and 10c,d. Shear strength is only due to friction angle, also for the silty sand sample 3-11. The shear strength angles at failure are ϕ'_f=50° (sample 1-11), 53° (2-11), 42° (3-11), while the residual angles are ϕ'_r=43° for both samples 1-11 and 2-11. Failure surfaces are well developed (Fig. 9c, sample 2-11), especially when the cell pressure is low.

Despite the grain size differences among the samples, the pyroclastic deposits show the same shear stress-strain behaviour.

6. Discussion

6.1 Transport and emplacement mechanisms of the Cotopaxi debris avalanche

The spatial distribution of facies types present in the Cotopaxi DA deposit indicates a general downstream progression from a stack of megablocks to a block-rich debris avalanche (Fig. 2). The further transition from debris avalanche to debris flow, and finally, to hyperconcentrated flow (Chillos Valley Lahar; Mothes et al., 1998) was not investigated in this work. The stratigraphic and textural characteristics at the outcrop scale of the Cotopaxi DA deposit contribute to the understanding of transport and emplacement processes that occurred in the volcanic debris avalanche after volcanic failure.

The Cotopaxi DA deposit shows evidence for three different flow behaviours as a function of the topography that the avalanche had encountered during emplacement and travel distance (Fig. 2): i) on the volcanic edifice; ii) in the Rio Pita valley floor; and iii) in distal marginal areas along the slopes of the adjacent volcanoes. In the proximal part (on the volcanic edifice) the debris avalanche slid predominantly confined by the valley E of the Ingaloma hill, emplacing the megablock facies. When the flow reached the break in slope at the base of the edifice, it strongly interacted with the pyroclastic substratum in the Rio Pita valley floor, generating the sheared facies. The main part of the flow spread laterally north-eastward in an unconfined fashion, forming a fan-shaped deposit of DA block facies on the Sincholagua volcano flanks.

In the megablock facies, single megablocks are monolithologic (Figs. 6b; 7a,c), suggesting the transport, as sliding blocks, of discrete segments of the volcano that are not thoroughly mixed. Overall, also the internal degree of fracturing and disaggregation is low (Figs. 7b,c), suggesting a scarce transport. All the megablocks are composed of massive lavas. The cluster of megablocks lodged against each other was formed as a consequence of the deceleration of the deposit at the break in slope, where larger material loses momentum and comes to rest. Inter-particle shear and frictional contact among DA megablocks may have occurred during this deceleration phase, as suggested by zones of inter-clast matrix composed of angular to subrounded lava fragments at the contact between megablocks (Fig. 4a). We interpret that the megablocks are the tail end of the debris avalanche, representing the summit portions of the collapsing edifice according to generally verified rockslide models (Bowman et al., 2012).

The mixed and sheared facies in the Cotopaxi DA deposit evidence that the pyroclastic substratum was entrained during avalanche transport. Rounded pyroclastic clasts and pumices in the mixed facies (Fig. 4d), forming the marginal part of the megablock facies E of Ingaloma hill, were likely derived from the banks of the Chalupas Ignimbrite (Fig. 2). This suggests that frictional contact may have occurred along the margins of the avalanche, and that the flow associated with the mixed facies was able to erode and was partially turbulent.

Along the Rio Pita valley, an array of deformation structures, including boudinage, folding, normal and thrust faulting, layer mixing, and injection structures are observed in the sheared facies (Figs. 2 and 7f). This facies comprises a complex interconnection of the DA megablocks and the Chalupas Ignimbrite. These structures suggest that the

dynamic conditions occurring during avalanche emplacement in the Rio Pita valley may have been influenced by the interaction with a poorly consolidated pyroclastic deposit on the valley floor, and by the presence of the elevated topographic obstacle of the southern slopes of Sicholagua volcano. The role of pore fluids in the development of the mixed and sheared facies is uncertain. The Chalupas Ignimbrite, occupying the valley floor of the Rio Pita, was probably partially saturated with ground water, which may have been involved in the dynamics of the sheared facies emplacement.

In the block facies, the DA deposit contains a large amount of blocks and minor matrix in all the depositional areas (Figs. 6c,d; 7d). This scarce presence of the matrix component could be related to a less energetic avalanche flow, due to a counterslope run-up of about 260 m, and/or to the absence of lubricating pyroclastic or other weak rocks involved as primary components of the avalanche. Indeed, pyroclastic components (pumices, glass shards, highly vesiculated particles) are absent in the megablock and block facies.

The effect of fragmentation on the DA transport mechanism is an open question (Haug et al., 2016). In general, at Cotopaxi, the blocks exhibit a decrease in maximum evident particle size with increasing distance along the presumed flow path. This reduction in particle size is probably the consequence of progressive fragmentation, disaggregation, and dilation processes that have occurred during the flow after the break in slope at the base of the volcano (Glicken, 1998). Following Bowman et al. (2012), an impulse velocity is generated by the fragmentation of the intact sliding blocks upon impact with the base of the volcanic edifice and among each other, which propels the DA front. Dilation and extension during transport (Schneider and Fisher, 1998; Thompson et al., 2009) are suggested by the textural characteristics of the

blocks (jigsaw cracks and jigsaw-fit fragmentation, crack width increase from centre to edges; Fig. 7e) and their subsequent dispersion, accompanied by intra-clast matrix injection. This mode of fragmentation accompanied by dilation of the flow implies a flow regime dominated by grain-collision stresses. Indeed, the majority of clasts are angular and blocky in shape, indicating absence of abrasion, whereas a very minor amount of clasts shows a weak rounding, suggesting that subordinate frictional stresses also occurred during transport.

The base of the Cotopaxi DA deposit was rarely exposed, and we were not able to describe and interpret the occurrence of the basal shearing layer commonly observed in other DA deposits at the contact with the run-out surface (Siebert, 1984; Schneider and Fischer, 1998).

6.2 The geotechnical characterization of the volcaniclastic materials

Grain size distribution provides information on the relative presence of fines, the fragmentation degree, and the influence of clast lithology. The grain size distribution of the DA deposit reveals a certain variability among coarser fractions, while the curves are nearly coincident for the fine fractions (silt and clay), which are the less represented, ranging 5-9%. The clay content is negligible, making the matrix cohesionless (Fig. 8a and Tab. 3). Another interesting observation is that despite both DA distal sample 7-14 and proximal sample 5-12 have the lowest sorting value (Tab. 3), they show a clear difference in the mean grain size, that accounts for the different degree of fragmentation and lithology. The similar high-content of sand in samples 7-14 and 4-12, that represent different lithofacies and emplacement distance, could be related to their clast lithology rather than only to the degree of disaggregation during

the flow, because they both have a significant amount of clasts composed of weak rocks (pyroclastic and hydrothermally altered, respectively).

A comparison with the grain size data available in literature revealed some similarities among the characteristics of Cotopaxi products and those of other volcanoes. Very few authors extended the analysis to coarser fractions. Among them, at the Tancitaro volcano, Morelli et al. (2010) obtained a larger variability in the coarse fraction of the deposit (3-17% cobbles, 19-50% gravel, 31-68% sand), while Roverato et al. (2015) at the Taranaki volcano, obtained a dominance of the gravel fraction (up to 86%). At the Shiveluch volcano, Belousov et al. (1999) obtained similar distributions for the block facies, although showing a wider range among samples (gravel 9-76%, 37% in average; sand 23-81%, 56% in average) and the mixed facies (gravel 23%, sand 67%). Grain size analyses performed by Glicken (1996) at Mt. S. Helens show an average 46% of gravel (over a range of 42-64%) and 45% of sand (range 29-51%). As concerns the fine fractions, all the authors (Glicken, 1996; Belousov et al., 1999; Cortez et al., 2010; Morelli et al., 2010; Roverato et al., 2015) observe a general small amount of fines (1-15%), with negligible to absent clay fraction (0-1.5%).

Our unit weight results (Tabs. 1 and 3) are comparable to the average dry unit weight (γ_d) determined by other authors, ranging 14-26 kN/m^3 (Glicken, 1996; Morelli et al., 2010; Roverato et al., 2015). Such values, lower than the mean density of the source rock, suggest a dilation of the material occurring during transport before deposition. As concerns the characterization of pyroclastic deposits carried out in this work, the samples were specifically chosen to be representative of the very different lithotechnical units cropping out in the northern flank of the volcano. This is crucial, were the poorly consolidated pyroclastic cover could lead to the formation of a gravity

driven instability phenomena like a granular flow or a debris flow. The results, in fact, show a strong variability in grain size distribution (Fig. 9b; Tab. 4). The best sorting, reflecting their depositional process, is observed for fallout-originated units (samples 3-11 and 8-14, Tab. 4), despite their very different mean grain value (d_m) and classification (SM, silty sand, and GW, well graded gravel with sand, related to an ash and an agglutinated scoria deposit, respectively). Porosity values (n) of the dry soil portion less than 8 mm are very high, reaching a maximum value of 44% in the agglutinated scoria deposit (sample 8-14, Tab. 4). As concern the determination of shear strength parameters, results are hardly found for volcanic DA deposits in the literature.

Our new results from consolidated drained triaxial compression tests point out that shear strength for cohesionless sandy materials is due to effective friction angle, which ranges 47-56° at failure (ϕ'_f,) and 40-43° for residual values (ϕ'_r) (Tab. 4). Morelli et al. (2010), who are the only others to have performed such analyses, provided an average value of effective friction angle of 33.5° over a range of 32-37°, determined by direct shear tests; such range is lower than our results at failure and more similar to residual values, and both works show a quite homogeneous behaviour over the set of tested samples.

The same analyses performed on specimens obtained from the pyroclastic deposit samples provided results similar to those of the DA deposit, because both sets considered the fine fraction less than 4.76 mm. Shear strength is only due to friction angle (also for the silty sand sample 3-11) and ranges 42-53° at failure, while residual value is 43°, delineating a similar shear stress-strain behaviour among the different

units. Failure surfaces are always well developed, especially when the cell pressure is low (Fig. 9c).

In general, the fundamental limit in characterising shear strength parameters by standard laboratory tests is related to the representativity of the sample (fractions <4.76 mm), which prevents from appreciating possible differences over the entire characteristic grain size curve of the deposit, neglecting the role of the coarser fraction in the global behaviour. In-situ direct shear tests on larger volumes, in the order of 30 dm^3 (Rotonda et al., 2009), are present, although very rare, in the literature. Although they minimize the problem of the representative volume, and are desirable, they do not solve it totally, especially in the case of wide total grain size distributions as observed at Cotopaxi.

6.3 Hazard related issues

The obtained results provide useful data for instability-related hazard studies, including volcanic debris avalanche and shallow landslides, and in particular for future investigations on the volcanic hazards of Cotopaxi.

Geotechnical characterizations on DA and pyroclastic deposits had never been done before on Cotopaxi. Although such analyses performed on a limited number of samples, these were chosen to be representative of the different lithotechnical units surveyed. These data, obtained from site-specific analyses based on standard geotechnical procedures and classification systems, signify an effort to characterize the volcano products also from a quantitative lithotechnical perspective. This, coupled with the new geological and volcanological detailed analyses, can improve the knowledge on the failure process and on the DA transport and emplacement dynamics,

which have produced the analysed deposits. This geotechnical characterization is also the essential premise to the development of adequate stability analyses of shallow landslide phenomena.

A thorough grain-size characterization including the coarser fractions is extremely relevant for a complete physical model of fragmentation during volcanic debris avalanche development and transport.

In general, and specifically for Cotopaxi, a small presence of fines and a negligible to absent amount of clay fractions suggest that no large portions of pyroclastic material nor/or hydrothermally altered rocks are involved in the failure process. Thus, hydrothermal alteration has not played a significant role in the Cotopaxi collapse, and the instability and DA triggering are to be ascribed to other factors.

Despite an average unit weight of pyroclastic material may be acceptable when simulating the transport process of an already mobilized pyroclastic succession, when investigating the failure process originating a landslide it is necessary to know the unit weight of each material where the shear surface would develop. This is also essential to prepare reconstituted samples for triaxial tests that best represent the behaviour of such original material.

Another important observation is that shear strength parameters that rule the triggering of collapse phenomena are mainly controlled by the fine fraction, which was here adequately tested and contextualised in the total grain size distribution.

7. Conclusions

The volcanological study of the 4.5 ka debris avalanche and younger pyroclastic deposits of the Cotopaxi volcano, coupled with the determination of their physical and

geotechnical parameters furnished the following results, which allow to understand the transport and emplacement mechanisms of the debris avalanche, to directly define the mechanical characteristic of these very peculiar materials, and to provide quantitative data applicable in debris flow hazard-related modelling and in stability evaluation analyses.

(a) The debris avalanche deposit includes four lithofacies types: megablock facies, block facies, mixed facies, and sheared facies, which correspond to different emplacement location and topography, flow regime, and role of substratum. The mega-block facies is composed of monolithologic blocks of the source volcano, >100 m in size, and it was restricted to the base of the volcano slopes, at short distance (7-8 km) from the cone summit. The block facies spread laterally as far as 35 km from the cone summit, forming an unconfined fan-shaped deposit.

(b) Different flow regimes prevailed during progressive phases of the debris avalanche transport. The debris avalanche transformed from a slide of megablocks, where inter-block shear and frictional contact may have occurred, to a block-bearing grain collision-dominated granular mass flow, with absence of abrasion and subordinate frictional stresses.

(c) A dynamic block fragmentation and dilation occurred during the debris avalanche transport. The decrease of the unit weight values of the materials and the gradual widening and splitting of jigsaw cracks, in the block facies, suggest that the maximum dilation component occurred along the avalanche flow. The increase in the degree of fragmentation (grain size reduction and jigsaw-fit textures) of the DA deposit with distance suggests that breakage of blocks increases progressively with the avalanche run-out. We suggest that the downslope-sliding intact source-blocks were fragmented

after impacting at the base of the volcano slope, with the base itself and each other. Then, the front of the sliding material accelerated because of the impulse velocity that was achieved by the breakage of the blocks. This dynamic fragmentation drove further run-out and the ability of the debris avalanche to climb up the counterslope flanks of the adjacent relieves.

(d) The interaction with the poorly consolidated pyroclastic substratum (Chalupas Ignimbrite) generated the mixed and sheared facies.

(e) The geotechnical results include a full-range grain size characterization, which complete the considerations on the facies features, reflecting their transport and depositional processes. The samples of the pyroclastic deposits show a broader variation in grain size distribution compared to those of the DA deposit, and a generally high porosity. The DA samples show a marked scarcity in the amount of the fine fraction, with negligible clay content.

(f) Consolidated drained triaxial compression tests show a quite similar shear stress-strain behaviour within each set of tested samples for both the DA and pyroclastic deposits, and point out that shear strength for the investigated cohesionless sandy materials is controlled by high values of effective friction angles. Especially for pyroclastic materials, failure surfaces are always well developed, indicating that the poorly consolidated pyroclastic cover could undergo failure leading to the formation of gravity-driven shallow instability phenomena.

(g) We retain that the shear strength parameters obtained from the consolidated drained triaxial compression tests are well representative of the fine-grained material portion, which exerts the control on the failure process and hosts the development of the shear surfaces leading to collapse.

(h) We retain that Cotopaxi's DA and pyroclastic deposits, for which this type of data were lacking, have now been reasonably characterized despite a quite limited number of samples were tested.

(i) Finally, this work underlies the general necessity for a site-specific, and interdisciplinary approach in the characterization of volcanic successions to provide reliable data for flank instability studies and simulations.

Acknowledgements

This study was financially supported by Italian MIUR–FIRB project "Relationship between large volcanic landslides and volcano evolution: consequences on geological hazard assessment and hydrogeological, geothermal and mineral exploration" through the grant RBAU01LHEE_003 to L. Vezzoli. F. Monti and A. Rupani are acknowledged for field and laboratory assistance. The authors thank M. Dapiaggi for X-ray powder diffraction analysis, performed at the X-Ray Power Diffraction Laboratory of the Earth Science Department of the University of Milan. Careful reviews by M. Hürlimann and an anonymous reviewer were greatly appreciated.

Appendix

Geotechnical standard methods used in this work (Tab. 2 and text):

ASTM D2487. Standard Practice for Classification of soils for engineering purposes (Unified Soil Classification System, USCS).

ASTM D422-63. Standard Test Method for Particle-Size Analysis of Soils. ASTM International, West Conshohocken, PA, www.astm.org.

ASTM D854. Standard Test Methods for Specific Gravity of Soil Solids by Water Pycnometer. ASTM International, West Conshohocken, PA, www.astm.org.

ASTM D4254. Standard Test Methods for Minimum Index Density and Unit Weight of Soils and Calculation of Relative Density. ASTM International, West Conshohocken, PA, www.astm.org.

ASTM D2216. Standard Test Methods for Laboratory Determination of Water (Moisture) Content of Soil and Rock by Mass. ASTM International, West Conshohocken, PA, www.astm.org.

ASTM D7181. Method for Consolidated Drained Triaxial Compression Test for Soils. ASTM International, West Conshohocken, PA, www.astm.org.

References

Adams, J., 1979. Gravel size analysis from photographs. J. Hydraul. Div. 10, 1247-1255.

Afrouz, A.A., 1992. Practical handbook of rock mass classification systems and modes of ground failure. CRC Press, London. 194 pp.

Aguilera, E., Pareschi, M.T., Rosi, M., Zanchetta, G., 2004. Risk from lahars in the northern valleys of Cotopaxi volcano, Ecuador. Natural Hazards 33, 161-189.

Andrade, S.D., van Wyk de Vries, B.V.W., 2010. Structural analysis of the early stages of catastrophic stratovolcano flank-collapse using analogue models. Bull. Volcanol. 72, 771-789.

Apuani, T., Corazzato, C., Cancelli, A., Tibaldi, A., 2005a. Physical and mechanical properties of rock masses at Stromboli: a dataset for volcano instability evaluation. Bull. Eng. Geol. Environ. 64, 419-431.

Apuani, T., Masetti, M., Uttini, A., Vezzoli, L., Corazzato, C., 2005b. Caratterizzazione geotecnica e modellazione numerica ad elementi distinti dei depositi della Sciara del Fuoco (Stromboli, Italia). Giornale di Geologia Applicata 2, 265-270.

Apuani, T., Masetti, M, Uttini, A., 2007. Debris slope stability analysis in an active volcano area. In: Malheiro, A.M., Nunes, J.C. (Eds.), Volcanic Rocks. Taylor and Francis Group, London, Proceedings of the International Workshop on Volcanic Rocks, 11th ISRM Congress, Ponta Delgada, Azores, Portugal, pp. 141-146.

Barberi, F., Caruso, F., Macedonio, P., Pareschi, M.T., Rosi, M., 1992. Reconstruction and numerical simulation of the lahar of the 1877 eruption of Cotopaxi volcano (Ecuador). Acta Vulcanol. 2, 35-44.

Barberi, F., Coltelli, M., Frullani, A., Rosi ,M., Almeida, E., 1995. Chronology and dispersal characteristics of recently (last 5000 years) erupted tephra of Cotopaxi (Ecuador): implications for long-term eruptive forecasting. J. Volcanol. Geotherm. Res. 69, 217-239.

Bell, F.G., 2000. Engineering properties of Soils and Rocks. 4th edition. Blackwell, Oxford.

Belousov, A., 1995. The Shiveluch volcanic eruption of 12 November 1964; explosive eruption provoked by failure of the edifice. J. Volcanol. Geotherm. Res. 66, 357–365.

Belousov, A., Belousova, M., Voight, B., 1999. Multiple edifice failure, debris avalanches and associated eruptions in the Holocene history of Shiveluch volcano, Kamchatka, Russia. Bull. Volcanol. 61, 324-342.

Bieniawski, Z.T., 1989. Engineering rock mass classifications: a complete manual for engineers and geologists in mining, civil, and petroleum engineering. John Wiley & Sons, New York, 257 pp.

Bernard, B., Andrade, D., 2011. Volcanes Cuaternarios del Ecuador Continental. IRD-IG-EPS, Quito.

Bigazzi, G., Coltelli, M., Hadler Neto, J.C., Osorio Araya, A.M., 1997. Provenance studies of obsidian artefacts using the fission-track analysis in South America: an overview. 49th Congreso Internacional del Americanistas, Quito, ARQ 14, 1-16.

Bowman, E.T., Take, W.A., Rait, K.L., Hann, C., 2012. Physical models of rock avalanche spreading behaviour with dynamic fragmentation. Can. Geotech. J. 49, 460-476.

Cáceres, B., 2005. Evaluación reciente del área del casquete glaciar del volcán Cotopaxi mediante la utilización de fotogrametría digital. XII Congreso Latinamericano de Geología, Quito, 4–6 May 2005.

Cortés, A., Macías, J.L., Capra, L., Garduño-Monroy, V.H., 2010. Sector collapse of the SW flank of Volcán de Colima, México: The 3600yr BP La Lumbre–Los Ganchos debris avalanche and associated debris flows. J. Volcanol. Geotherm. Res. 197, 52-66.

Crandell, D.R., Miller, C.D., Glicken, H.X., Christiansen, R.L., Newhall, C.G., 1984. Catastrophic debris avalanche from ancestral Mount Shasta volcano, California. Geology 12, 143-146.

Crosta, G.B., Imposimato, S., Roddeman, D., Chiesa, S., Moia, F., 2005. Small fast-moving flow-like landslides in volcanic deposits: the 2001 Las Colinas Landslide (El Salvador). Eng. Geol. 79, 185–214.

del Potro, R., Hürlimann, M., 2008. Geotechnical classification and characterisation of materials for stability analyses of large volcanic slopes. Eng. Geol. 98, 1- 17.

Di Muro, A., Rosi, M., Aguilera, A., Barbieri, R., Massa, G., Mundula, F., Pieri, F., 2008. Transport and sedimentation dynamics of transitional explosive eruption columns: The example of the 800 BP Quilotoa Plinian eruption (Ecuador). J. Volcanol. Geotherm. Res. 174, 307–324.

Dinis da Gama, C., Ribeiro e Sousa, L., (Eds.), 2002. Workshop on Volcanic Rocks, ISRM International Symposium on Rock Engineering for Mountainous Regions, Eurock, Funchal, November 25-28th.

Esu, F., 1977. Behaviour of slopes in structurally complex formations. Proceedings of the international symposium on the geotechnics of structurally complex formations, 2, 292-304.

Evangelista, A., Picarelli, L., 1998. The geotechnics of hard soils-soft rocks. Volume 2, AA Balkema. pp. ix+-591.

Fiorini, E., Tibaldi, A., 2012. Quaternary tectonics in the central Interandean Valley, Ecuador: Fault-propagation folds, transfer faults and the Cotopaxi Volcano. Global Planet. Change 90-91, 87–103.

Folk, R.L., Ward, W.C., 1957. Brazos river bar: a study of significance of grain size parameters. J. Sedim. Petrol. 27, 3-26.

Franz, W.J., Voight, B., 1995. Shear strength of granular debris from the Osceola Mudflow, Mount Rainier Volcano, Washington. EOS Abstracts Am. Geophys. Union, F651.

Friedmann, S.J., 1997. Rock-avalanche elements of the Shadow valley basin, eastern Mojave desert, California: processes and problems. J. Sedim. Res. 67, 792-804.

Glicken, H., 1991. Sedimentary architecture of large volcanic-debris avalanches. In: Smith, G.A., Fisher, R.V. (Eds.), Sedimentation in Volcanic Settings. SEPM Spec. Publ., vol. 45, pp. 99-106.

Glicken, H., 1996. Rockslide-debris avalanche of May 18, 1980, Mount St. Helens volcano, Washington. USGS Open-file Report, 96-677, Cascades Volcano Observatory, Vancouver, 90 pp.

González de Vallejo, L.I., Hijazo Ramiro, T., Ferrer Gijón, M., 2008. Engineering geological properties of the volcanic rocks and soils of the Canary Islands. Soils and Rocks 31, 3-13.

Hammersley, L., 2003. The Chalupas caldera. PhD Thesis, Berkeley, California.

Hall, M.L., Mothes, P.A., Hidalgo, S., 2005. Volcanic history of Cotopaxi Volcano, Ecuador. In folio geological map. Instituto Geofisico, Escuela Politécnica Nacional, Quito.

Hall, M., Mothes, P., 2008a. The rhyolitic-andesitic eruptive history of Cotopaxi volcano, Ecuador. Bull. Volcanol. 70, 675–702.

Hall, M.L., Mothes, P.A., 2008b. Quilotoa volcano, Ecuador: an overview of young dacitic volcanism in a lake-filled caldera. J. Volcanol. Geotherm. Res. 176, 44–55.

Hall, M., von Hillebrandt, C., 1988. Mapa de los Peligros Volcánicos Potenciales Asociados con el Volcán Cotopaxi (1:50,000). Quito, Instituto Geofísico, Escuela Politécnica Nacional.

Haug, Ø.T., Rosenau, M, Leever, K., Oncken, O., 2016. On the energy budgets of fragmenting rockfalls and rockslides: Insights from experiments. J. Geophys. Res. Earth Surface 121, 1310-1327.

Hickey, J., Gottsmann, J., Mothes, P., 2015. Estimating volcanic deformation source parameters with a finite element inversion: The 2001–2002 unrest at Cotopaxi volcano, Ecuador. J. Geophys. Res. 120, 1473–1486.

Hoek, E., 2001. Big tunnels in bad rock. Journal of Geotechnical and Geoenvironmental Engineering, 127, 726-740.

Hoek, E., Carranza-Torres, C., Corkum, B., 2002. Hoek–Brown Criterion. Proc. NARMS-TAC Conference, Toronto, 1, 267–273.

Hürlimann, M., Ledesma, A., Martí, J., 2001. Characterisation of a volcanic residual soil and its implications for large landslide phenomena: application to Tenerife, Canary Islands. Eng. Geol. 59, 115–132.

Iverson, R.M., Schilling, S.P., Vallance, J.W., 1998. Objective delineation of lahar-inundation hazard zones. Geol. Soc. Am. Bull. 110, 972–984.

Jackson, J.A., Bates, R.L., 1997. Glossary of Geology. Fourth Edition, Am. Geological Inst., 769 pp.

Jordan, E., 1983. Die Vergletscherung des Cotopaxi, Ecuador. Zeitsch. Gletscherkunde und Glaziologie 19, 73-102.

Kelfoun, K., Druitt, T.H., 2005. Numerical modelling of the emplacement of Socompa rock avalanche, Chile. J. Geophys. Res. 110, B12202.

Kellerhals, R., Bray, D.I., 1971. Sampling procedures for coarse fluvial sediments. J. Hydraul. Eng., 97, 1165-1180.

Lipman, P.W., Mullineaux, D.R. (Eds.), 1981. The 1980 eruptions of Mount St. Helens, Washington. US Geological Survey.

Longchamp, C., Abellan, A., Jaboyedoff, M., Manzella, I., 2015. 3-D models and structural analysis of analogue rock avalanche deposits: a kinematic analysis of the propagation mechanism. Earth Surf. Dynam. Discuss. 3, 1255–1288.

Ludovico Marques, M.A., Delgado Rodrigues, J., 2002. Consolidation of volcanic tuffs. Some physical and mechanical properties. In: Dinis da Gama, C., Ribeiro e Sousa, L. (Eds.), Workshop on Volcanic Rocks, ISRM International Symposium on Rock Engineering for Mountainous Regions, Eurock, 37–44.

Malheiro, A.M., Nunes, J.C., (Eds), 2007. Volcanic Rocks. Proceedings of the International Workshop on Volcanic Rocks, ISRM Congress, Ponta Delgada, Azores, Taylor and Francis Group, London, UK.

Marinos, P., Hoek, E., 2000. GSI: a geological friendly tool for rock mass strength estimation. Proceeding GeoEng2000, IAEG, ISSFME, ISRM, Melbourne, Australia.

Marinos, P., Marinos, V., Hoek, E., 2007. Geological Strength Index (GSI). A characterization tool for assessing engineering properties for rock masses. Underground works under special conditions. Taylor and Francis, Lisbon, 13-21.

Mehl, K.W., Schmincke, H.U., 1999. Structure and emplacement of the Pliocene Roque Nublo debris avalanche deposit, Gran Canaria, Spain. J. Volcanol. Geotherm. Res. 94, 105-134.

Miller, C.D., Mullineaux, D.R., Hall, M.L., 1978. Reconnaissance map of potential volcanic hazards from Cotopaxi volcano, Ecuador. U.S. Geol. Survey Map, I-1072.

Molina, I., Kumagai, H., Garcia-Aristizabal, A., Nakano, M., Mothes, P., 2008. Source process of very long-period events accompanying long-period signals at Cotopaxi Volcano, Ecuador. J. Volcanol. Geotherm. Res. 176, 119–133.

Moon, V.G., 1993. Geotechnical characteristics of ignimbrite, a soft pyroclastic-rock type. Eng. Geol. 35, 33–48.

Moon, V., Bradshaw, J., Smith, R., de Lange, W., 2005. Geotechnical characterisation of stratocone crater wall sequences, White Island Volcano, New Zealand. Eng. Geol. 81, 146–178.

Morelli, S., Garduño-Monroy, V.H., Gigli, G., Falorni, G., Rocha, E.A., Casagli, N., 2010. The Tancitaro debris avalanche: characterization, propagation and modeling. J. Volcanol. Geotherm. Res. 193, 93-105.

Mothes, P., 1992. Lahars of Cotopaxi volcano, Ecuador: hazard and risk evaluation. In: McCall, G.J.H., Scott, S.C. (Eds.), Geohazards, natural and man-made. Chapman and Hall, London, pp. 53-64.

Mothes, P., 2006. Cotopaxi volcano and the surrounding valleys. Intra-meeting field trip guide. Cities on Volcanoes 4 IAVCEI, Quito, Ecuador (2006), 30 pp.

Mothes, P., Hall, M.L., Janda, R.J., 1998. The enormous Chillos Valley Lahar: an ash-flow-generated debris flow from Cotopaxi volcano, Ecuador. Bull. Volcanol. 59, 233-244.

Mothes, P., Hall, M., Andrade, D., Samaniego, P., Pierson, T., Ruiz, G., Yepes, H., 2004. Character, stratigraphy and magnitude of historical lahars of Cotopaxi volcano, Ecuador. Acta Volcanol. 16, 85–107.

Olalla, C., Hernandez, L.E., Rodriguez-Losada, J.A., Perucho, A., Gonzalez-Gallego, J. (Eds.), 2010. Volcanic Rock Mechanics. Rock Mechanics and Geo-engineering in Volcanic Environments. 3rd International Workshop, Pueblo de la Cruz, Tenerife (Canary Islands), Spain, 31 May-1 June 2010. Taylor and Francis Group, London.

Olivera, R., 1993. The engineering geology of weak rock. In: Cripps, J.C., Coulthard, J.M., Culshaw, M.G., Forster, A. (eds.), Weak rock materials. Eng. Group, Geol. Soc. Spec. Publ., 8, 5–15.

Okubo, C.H., 2004. Rock mass strength and slope stability of the Hilina slump, Kilauea volcano, Hawai'i. J. Volcanol. Geotherm. Res. 138, 43–76.

Palmer, B.A., Alloway, B.V., Neall, V.E., 1991. Volcanic-debris-avalanche deposits in New Zealand: Lithofacies organization in unconfined, wet-avalanche flows. In: Fisher, R.V., Smith, G.A. (Eds), Sedimentation in volcanic setting. SEPM Spec. Pub., vol. 45, pp. 89-98.

Patra, A., Bauer, A., Nichita, C.C., Pitman, E.B., Sheridan, M.F., Bursik, M.I., Rupp, B., Webber, A., Stinton, A.J., Namikawa, L., Renschler, C., 2005. Parallel adaptive numerical simulation of dry avalanches over natural terrain. J. Volcanol. Geotherm. Res. 139, 1–21.

Pistolesi, M., Rosi, M., Cioni, R., Cashman, K.V., Rossotti, A., Aguilera, E., 2011. Physical volcanology of the post-twelfth-century activity at Cotopaxi volcano, Ecuador: Behavior of an andesitic central volcano. Geol. Soc. Am. Bull. 123, 1193–1215.

Pistolesi, M., Cioni, R., Rosi, M., Cashman, K.V., Rossotti, A., Aguilera, E., 2013. Evidence for lahar-triggering mechanisms in complex stratigraphic sequences: The post-twelfth century eruptive activity of Cotopaxi Volcano, Ecuador. Bull. Volcanol. 75, 1–18.

Pistolesi, M., Cioni, R., Rosi, M., Aguilera, E., 2014. Lahar hazard assessment in the southern drainage system of Cotopaxi volcano, Ecuador: Results from multiscale lahar simulations. Geomorphology 207, 51–63.

Rolo, R., Bommer, J.J., Houghton, B.F., Vallance, J.W., Berdousis, P., Mavrommati, C., Murphy, W., 2004. Geologic and engineering characterization of Tierra Blanca pyroclastic ash deposits. In: Rose, W.I., Bommer, J.J., Lopez, D.L., Carr, M.J., Major, J.J. (Eds.), Natural Hazards in El Salvador. Geol. Soc. Am. Spec. Papers, 375, 55–68.

Rotonda, T., Tommasi, P., Boldini, D., 2009. Geomechanical characterization of the volcaniclastic material involved in the 2002 landslides at Stromboli. J. Geotech. Geoenviron. Eng. 136, 389-401.

Rotonda T., Cecconi, M., Silvestri, F., Tommasi, P. (Eds), 2016. Volcanic Rocks and Soils. Proceeding of the Workshop on Volcanic Rocks and Soils, ISRM Specialised Conference, Ischia, Taylor and Francis Group, London.

Roverato, M., Cronin, S., Procter, J., Capra, L., 2015. Textural features as indicators of debris avalanche transport and emplacement, Taranaki volcano. Geol. Soc. Am. Bull. 127, 3-18.

Schaefer, L.N., Oommen, T., Corazzato, C., Tibaldi, A., Escobar-Wolf, R., Rose W.I., 2013. An integrated field-numerical approach to assess slope stability hazards at volcanoes: the example of Pacaya, Guatemala. Bull. Volcanol. 75, 720.

Schaefer, L.N., Kendrick, J.E., Oommen, T., Yan Lavallée, Y., Chigna G., 2015. Geomechanical rock properties of a basaltic volcano. Frontiers in Earth Science, doi: 10.3389/feart.2015.00029

Schneider, J.L., Fisher, R.V., 1998. Transport and emplacement mechanisms of large volcanic debris avalanches: evidence from the northwest sector of Cantal Volcano (France). J. Volcanol. Geotherm. Res. 83, 141-165.

Schuster, R.L., Crandell, D.R., 1984. Catastrophic debris avalanches from volcanoes. IV International Symposium on landslides proceedings, Vol. 1, pp. 567-572.

Shea, T., van Wyk de Vries, B.V., 2008. Structural analysis and analogue modeling of the kinematics and dynamics of rockslide avalanches. Geosphere 4, 657-686.

Siebert, L., 1984. Large volcanic debris avalanches: characteristics of source areas, deposits, and associated eruptions. J. Volcanol. Geotherm. Res. 22, 163-197.

Smith, G.N., 1982. Elements of Soil Mechanics for Civil and Mining Engineers. Granada, Monograph. Granada Publishing Limited, London, 493 pp.

Smyth, M., 1991. Movement and emplacement mechanisms of the Río Pita volcanic debris avalanche and its role in the evolution of Cotopaxi volcano. PhD Thesis, Univ Aberdeen, Scotland.

Smyth, M.A., Clapperton, C.M., 1986. Late quaternary volcanic debris avalanche at Cotopaxi, Ecuador. Revista Centro Interamericano de Fotointerpretation, Bogotà, 11, 24-38.

Sosio, R., Crosta, G.B., Hungr, O., 2012. Numerical modeling of debris avalanche propagation from collapse of volcanic edifices. Landslides 9, 315-334.

Thomas, M.E., Petford, N., Bromhead, E.N., 2004. Volcanic rock-mass properties from Snowdonia and Tenerife: implications for volcano edifice strength. J. Geol. Soc. London 161, 939-946.

Thompson, N., Bennett, M.R., Petford, N., 2009. Analyses on granular mass movement mechanics and deformation with distinct element numerical modeling: implications for large-scale rock and debris avalanches. Acta Geotechnica 4, 233-247.

Tibaldi, A., Bistacchi, A., Pasquarè F.A., Vezzoli, L., 2006. Extensional tectonics and volcano lateral collapses: insights from Ollague volcano (Chile-Bolivia) and analogue modelling. Terra Nova 18, 282–289.

Ui, T., 1983. Volcanic dry avalanche deposits - identification and comparison with nonvolcanic debris stream deposits. J. Volcanol. Geotherm. Res. 18, 135–150.

Ui, T., Glicken, H., 1986. Internal structural variations in a debris-avalanche deposit from ancestral Mount Shasta, California, USA. Bull. Volcanol. 48, 189-194.

van Wyk de Vries, B., Davies, T., 2015. Landslides, debris avalanches, and volcanic gravitational deformation. In: McNutt, S.R., Stix, J., Rymer, H., Houghton, B.,

Sigurdsson, H. (Eds.),The Encyclopedia of Volcanoes, Second Edition, Elsevier, 665-685.

Voight, B., Glicken, H., Janda, R.J., Douglass, P.M., 1981. Catastrophic rockslide avalanche of May 18. In: Lipman, P.W., Mullineaux, D.R. (Eds.), The 1980 eruptions of Mount St. Helens. U.S. Geological Survey Prof. Paper, 1250, pp. 347-377.

Voight, B., Janda, R.J., Glicken, H., Douglass, P.M., 1983. Nature and mechanics of the Mount St-Helens rockslide-avalanche of 18 May 1980. Geotechnique 33, 243–273.

Watters, R.J., Zimbelman, D.R., Bowman, S.D., Crowley, J.K., 2000. Rock mass strength assessment and significance to edifice stability, Mount Rainier and Mount Hood, Cascade Range Volcanoes. Pure and Applied Geophysics 157, 957–976.

Wolf, T., 1904. Cronica de los fenomenos volcanicos y terremotos del Ecuador, con algunas noticias sobre otros paises del la America Central y Meridional, desde 1533 a 1797. Annales Univ Central, Quito, 8, 1-120.

Yoshida, H., 2013. Decrease of size of hummocks with downstream distance in the rockslide-debris avalanche deposit at Iriga volcano, Philippines: similarities with Japanese avalanches. Landslides 10, 665–672.

Figure Captions

Figure 1 - (a) Location of the Cotopaxi volcano in the Ecuadorian Andes. EC = Eastern Cordillera; IV = Interandean Valley; WC = Western Cordillera. Redrawn after Bernard and Andrade (2011) and Fiorini and Tibaldi (2012). The inset shows the location of Figure 1a in the regional context. (b) Geological map of the Cotopaxi volcano, redrawn after Hall et al. (2005) and Hall and Mothes (2008a). The extent of the debris avalanche deposit is inferred from our original field survey. Contour lines in metres. Box shows the location of Figure 2.

Figure 2 - Geological map of the northern flank of the Cotopaxi volcano (location in Fig. 1b) showing the areal extent of the 4.5 ka old debris avalanche deposit recognized in this study. The younger tephra and paleosols strata blanketing the DA deposit are omitted. Symbols and adjacent numbers identify sites where stratigraphic data and volcaniclastic samples were collected. As a base, the 1:50,000 topographic map of Instituto Geografico Militar, Quito, Ecuador (Sincholagua sheet, NIII-D3, 3992-III, Serie-J721, year 1989, second edition). Contour lines are every 40 m.

Figure 3 – (a) Synthetic stratigraphic logs for the pyroclastic deposits emplaced after the 4.5 ka lateral collapse and debris avalanche (DA) of Cotopaxi as in previous literature. Not to scale. Labels identifying key tephra beds from Barberi et al. (1995) and Pistolesi et al. (2011). (b) Stratigraphic sections measured in this work, showing the tephra layers correlation and stratigraphic position of samples. Tephra

nomenclature is from Barberi et al. (1995) and Pistolesi et al. (2011) as in Figure 3a. Section locations are marked in Figure 2.

Figure 4 – Photographs of the samples analysed. The scale bar is 1-m long. (a) Sample 4-12 represents the inter-clast matrix in the megablock facies. Larger fragments are composed of andesitic lavas with phenocrysts of argillified plagioclase, smaller fragments comprise white argillified materials. (b) Sample 5-12 is a monogenetic clast-supported breccia composed of angular clasts, decimetre in size, which represents the intra-clast matrix of the megablock facies. (c) Sample 6-12 is the outer, brecciated part of a megablock. (d) Sample 7-14 is composed of a polygenetic, matrix-supported breccia with vitric-lithic matrix, and represents the mixed facies. (e) Sample 2-11 comprises a massive bed of agglutinated, black and oxidized scoriaceous lapilli and coarse bombs. (f) Sample 3-11 is composed of a poorly consolidated, well-sorted vitric ash. The upper part of the ash bed is weakly pedogenized.

Figure 5 – (a) The representativeness of laboratory tests on collected samples and in situ-analyses with respect to the total grain size distribution of the DA and pyroclastic deposits. Grain size fields according to ASTM (American Society for Testing and Materials). USCS = unified Soil Classification System. (b) In situ grain size analysis of the sample fraction >128 mm was performed by image analysis on a 1 m^2 grid on the outcrop. (c) In situ grain-size analysis of the sample fraction 128-8 mm was performed with callipers, an 8 mm sieve, and a mechanical steelyard.

Figure 6 – (a) Photo of the hummocky surface of the 4.5 ka old Cotopaxi volcanic debris avalanche deposit in the Rio Pita valley and on the southern slopes of Sincholagua Volcano. The uppermost hummocks reach about 4020 m asl with a run up of about 260 m. (b) Photo of an asymmetric hummock made from a single, relatively intact, megablock of lava representing a segment of the pre-rupture volcanic flank that was transported for a 9.3 km distance without disaggregating. The hummock is 400 m long and 150 m high. The megablock is mantled by a stratified cover of tephra and paleosol beds (the hatched white line indicates the contact). In the foreground is the deposit of the 1877 scoria and debris flow. (c) A distal hummock in the Rio Carcelen at about 20 km from the volcano summit, showing a core of DA block facies and a thick cover made by younger tephra (hatched white line at the contact) that mimic the hummock's surface morphology. (d) The basal contact of the DA block facies deposit with the Chalupas Ignimbrite (CI) along the Rio Carcelen valley.

Figure 7 - Textures of the debris avalanche facies. (a) A megablock composed of fractured but coherent lava core that was gradually transformed in a breccia. (b) Detail of the megablock of Figure 7a showing the lava core pervasively fractured by a network of jigsaw cracks. (c) Detail of the megablock of Figure 7a showing the transition from the intact lava core, with well-preserved slaty texture (S), to a jigsaw-crack (JC) texture and, finally, to a jigsaw-fit (JF) breccia. (d) The interior of a hummock with block facies. Note the scarce presence of the inter-clast matrix component. Encircled person for scale. (e) A typical fractured and jigsaw-fit lava block in the DA block facies of Figure 7d. The cracks widened, increasing from the centre to the edge, and are injected by intra-clast matrix, suggesting an incipient dilatation and a

partial disaggregation of the block. Hammer for scale. (f) The sheared facies, showing slabs of Chalupas Ignimbrite (CI) and andesitic scoriaceous lavas (Ls) that are folded and faulted together. The lava slab is stretched, deformed in a brittle behaviour with low-angle extensional faults, and sheared in flame structures. T = younger tephra and debris flow deposits.

Figure 8 - Particle size distribution of the studied deposits according to ASTM (American Society for Testing and Materials). (a) debris avalanche (DA) deposit. (b) pyroclastic (PY) deposits.

Figure 9 –Principal stress difference (σ_1'-σ_3', deviatoric stress) and change in volume ($\Delta V/V_c$) versus axial strain (ε) curves from Consolidated Drained Triaxial Compression Test on (a) debris avalanche (DA) samples (6-12 and 7-14) and (b) pyroclastic deposits (PY) samples (2-11 and 3-11). Pictures (c) show the specimens of DA sample 7-14, tested at σ_3=154 kPa (left), and PY sample 2-11, tested at σ_3 = 152 kPa (right), at the end of the test (with and without the membrane), showing a well-developed shear zone.

Figure 10 – Shear stress (τ') versus normal stress (σ') graph and Mohr stress circles at failure from Consolidated Drained Triaxial Compression Test on samples 4-12 (DA) (a) and 2-11 (PY) (c). ϕ' = effective shear strength angle. Centre of the Mohr stress circle (s' = one half the sum of the major and minor effective principal stress) versus radius of the Mohr stress circle (t' = one half the sum of the major and minor effective principal stress) graph obtained from all the DA (b) and PY (d) samples.

Figure 11 - (a) The western scarp of the Quebrada Yanasacha showing the lithological discontinuity between lavas and younger pyroclastic deposits on the northern slope of the Cotopaxi cone. The black-and-red bed in the middle of the scarp comprises agglutinated scoriaceous lapilli and bombs and is represented by sample 2-11. (b) Photo of the stratigraphic section of the Quebrada Yanasacha at 3960 m asl (number 3 in Figs. 2 and 3b). The stratigraphic location of sample 2-11 is indicated. The scale bar is 1 m long. (c) Photo of the stratigraphic section along the road toward the Refugio J.F. Riva at 4230 m asl (number 2 in Figs. 2 and 3b). The location of samples 3-11 and 8-14 is depicted. Hammer for scale. (d) Photo of the stratigraphic section at old Refugio Arma National at 4550 m asl (number 4 in Figs. 2 and 3b). This log shows the detail of the upper part of the pyroclastic sequence composed of loose pumice and scoria lapilli and ash layers where sample 1-11 was collected. These well-stratified beds are fall-out deposits related to historical explosive eruptions, and they are partially reworked for syn-eruptive small granular flows. Hammer for scale.

Table captions

Table 1 – Location and characteristics of the Cotopaxi samples.

Table 2 – Summary of in situ and laboratory analyses performed on the Cotopaxi samples.

Table 3 – Grain size analyses data and physical parameters of the debris avalanche deposit (DA).

Table 4 – Grain size analyses data and physical parameters of the pyroclastic deposits (PY).

Table 1. Location and characteristics of the Cotopaxi samples

Sample	Locality	m asl	Coordinates*	Lithofacies	W_n (kg)	V_n (dm^3)	γ_n (N/m^3)	φ (°)
Debris avalanche deposit								
4-12	Quebrada Victor Puñuna	3944	0787208N 9932304E	Megablock facies	11.5	4.5	25.09	43
5-12	Quebrada Victor Puñuna	3952	0787252N 9930675E	Block facies	11.0	4.2	25.68	47
6-12	Quebrada Victor Puñuna	3848	0787273N 9933255E	Megablock facies	13.0	5.2	24.50	41
7-14	Rio Pia, left bank	3712	0786815N 9936671E	Mixed facies	7.0	2.65	25.87	39
Pyroclastic deposits								
1-11	Road toward Refugio J.F. Riva	4555	0785560N 9927885E	Stratified lapilli and coarse ash	16.5	9.0	17.93	47
2-11	Road toward Refugio J.F. Riva	4417	0785791N 9928413E	Spatter and scoria breccia	7.25	4.0	17.74	38
3-11	Road toward Refugio J.F.	4163	0785274N 9929820E	Massive fine ash	9.5	6.65	14.01	45

	Riva							
8-14	Road toward Refugio J.F. Riva	4163	0785274N 9929820E	Pumice lapilli	4.5	4.35	10.09	30

* Coordinates in metres, UTM 17, WGS 84. W_n = total sample mass; V_n = in-situ sample volume; γ_n = in-situ natural unit weight; φ = in-situ angle of repose.

Table 2. Summary of in situ and laboratory analyses performed on the Cotopaxi samples

	Materials	**Method/standard reference**
In situ analyses		
Detailed topographic profile	volcano northern flank	GPS measurement
Particle size distribution	>128 mm fraction	Digital image analysis
Particle size distribution	128-8 mm fraction	Calliper and sieving analyses
Laboratory analyses		
Particle size distribution	8-0.074 mm fraction	Sieving analysis (ASTM D422-63)
Particle size distribution	<0.074 mm fraction	Hydrometer analysis (ASTM D422-63)
Particle apparent specific gravity (G_s)	<8 mm fraction	Water pycnometer (ASTM D854)
Bulk specific gravity (G_{sa})	<0.074 mm fraction	Water pycnometer (ASTM D854)
Minimum and maximum	<8 mm fraction	ASTM D4254

void index ratio (e_{min}, e_{max}), porosity (n_{min}, n_{max}) and density ($\gamma_{d\,min}$, $\gamma_{d\,max}$) calculation		
Water content (w)	<8 mm fraction	ASTM D2216
Mineralogical composition	<0.074 mm fraction	X-Ray diffractometric analysis
Shear strength parameters: cohesion (c) and friction angle (ϕ)	<4.76 mm fraction	Consolidated drained triaxial compression test (ASTM D7181)

ASTM codes as in Appendix

Table 3. Grain size analyses data and physical parameters of the debris avalanche deposit (DA).

DA sample	4-12	5-12	6-12	7-14
All soil fractions (cfr. Fig. 9a)				
Boulders %	4	28	0	12
Cobbles %	24	21	26	7
Gravel %	23	22	42	30
Sand %	40	23	27	43
Silt %	9	6	5	8
Clay %	<0.01	<0.01	<0.01	<0.01
Soil portion d < 75 mm				
Gravel %	31.0	43.4	57.6	44.9
Sand %	57.3	45.5	36.5	46.0
Fine fraction %	11.7	11.1	6.0	9.1
Cu	31	77	118	71
Cc	1	4	1	0
USCS group name	Poorly graded sand with	Poorly graded sand with	Poorly graded gravel with	Poorly graded sand with

		gravel and silt	gravel and silt	sand and silt	gravel and silt
USCS	group simbol	SP-SM	SP-SM	GP-GM	SP-SM
Sedimentological parameters					
sorting	phi	3.87	3.26	3.74	3.26
d_m	phi	-1.60	-3.41	-3.47	-0.97
Soil portion d < 0.074 mm					
G_{sa}	kN/m^3	24.11	25.00	26.62	25.13
Soil portion d < 8 mm					
G_s	kN/m^3	18.98	18.60	22.46	16.34
w	%	18.54	8.65	3.76	11.83
$\gamma_{d\ min}$	kN/m^3	11.79	13.84	15.21	13.67
$\gamma_{d\ max}$	kN/m^3	15.14	17.52	18.62	16.66
n_{min}		0.20	0.06	0.17	-
n_{max}		0.38	0.26	0.32	0.16
e_{min}		0.25	0.06	0.21	-
e_{max}		0.61	0.34	0.48	0.20

Cu = coefficient of uniformity; Cc = coefficient of curvature; USCS = Unified Soil Classification System; d_m = average particle diameter; other abbreviations as in Table 2.

Table 4. Grain size analyses data and physical parameters of the pyroclastic deposits (PY).

PY sample		1-11	2-11	3-11	8-14
Soil portion d < 75 mm (cfr. Fig. 9b)					
Gravel %		32	51	0	81
Sand %		62	43	77	18
Fine fraction %		6	6	23	1
Cu		7.06	73.93	3.21	7.08
Cc		0.69	0.22	1.13	1.86
USCS	group name	Poorly graded sand with gravel and silt	Poorly graded gravel with sand and silt	Silty sand	Well-graded gravel with sand
USCS	group simbol	SP-SM	GP-GM	SM	GW
Sedimentological parameters					
sorting	phi	2.9	3.1	1.1	1.4
d_m	phi	0.4	-1.6	3.0	-3.4
Soil portion d < 0.074 mm					

G_{sa}	kN/m^3	18.99	14.95	19.54	12.60
Soil portion d < 8 mm					
G_s	kN/m^3	-	-	25.20	-
w	%	10.18	17.00	18.20	20.56
$\gamma_{d\ min}$	kN/m^3	13.09	8.78	-	7.03
$\gamma_{d\ max}$	kN/m^3	15.55	11.17	-	9.39
n_{min}		0.18	0.25	-	0.26
n_{max}		0.31	0.41	-	0.44
e_{min}		0.22	0.34	-	0.34
e_{max}		0.45	0.70	-	0.79

Abbreviations as in Tables 2 and 3.

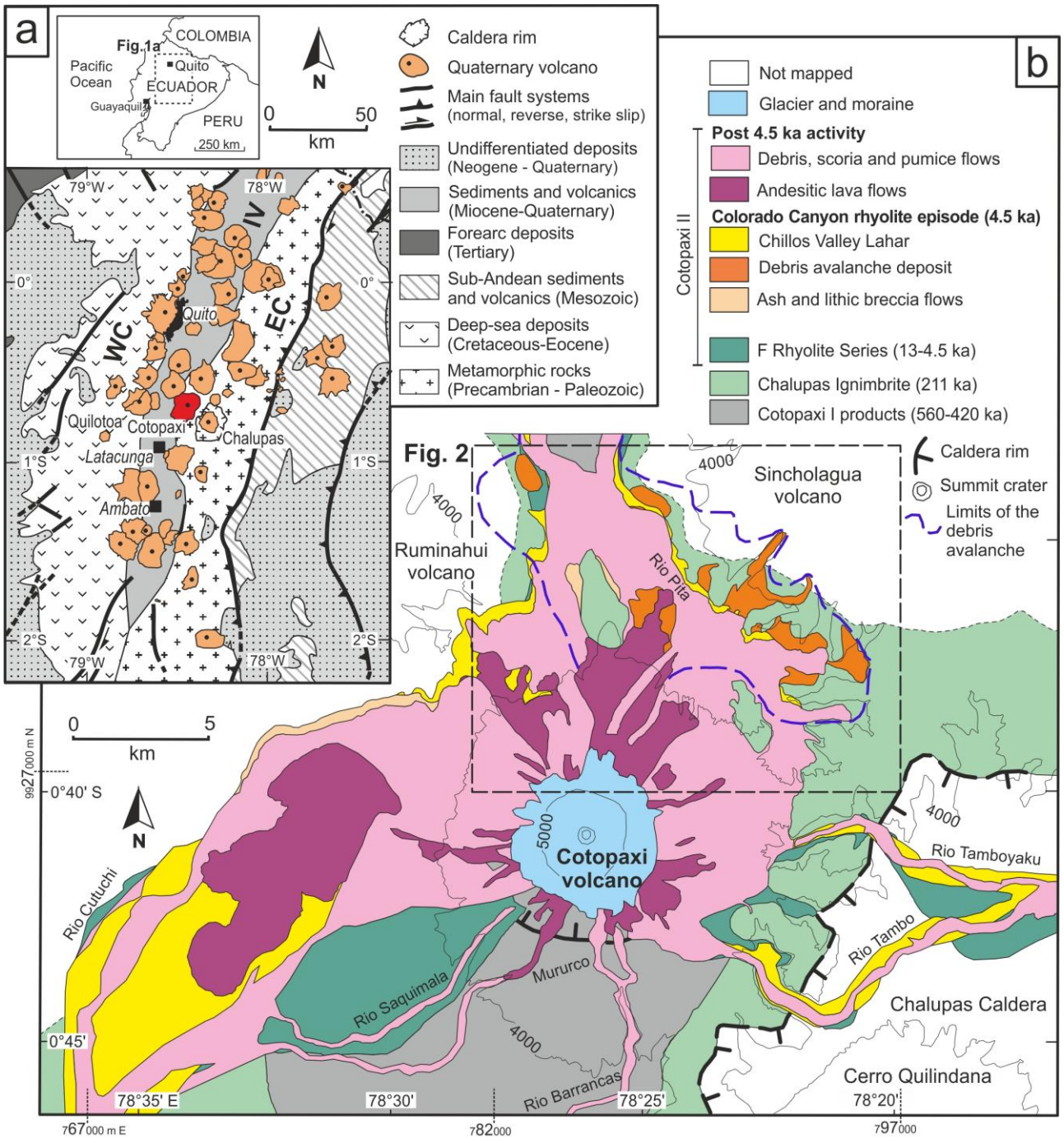

Vezzoli et al. - Cotopaxi - Fig. 1

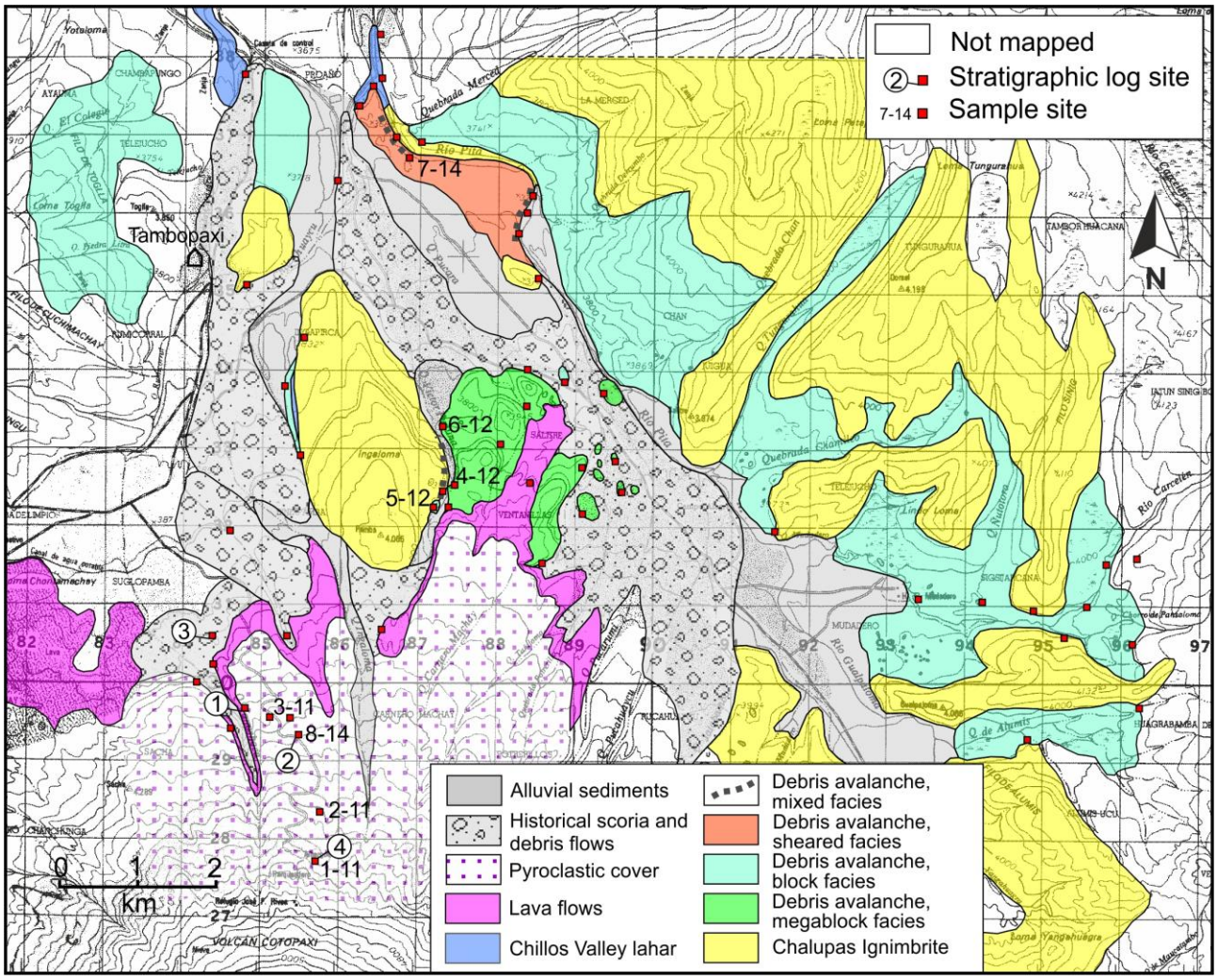

Vezzoli et al. - Cotopaxi - Fig. 2

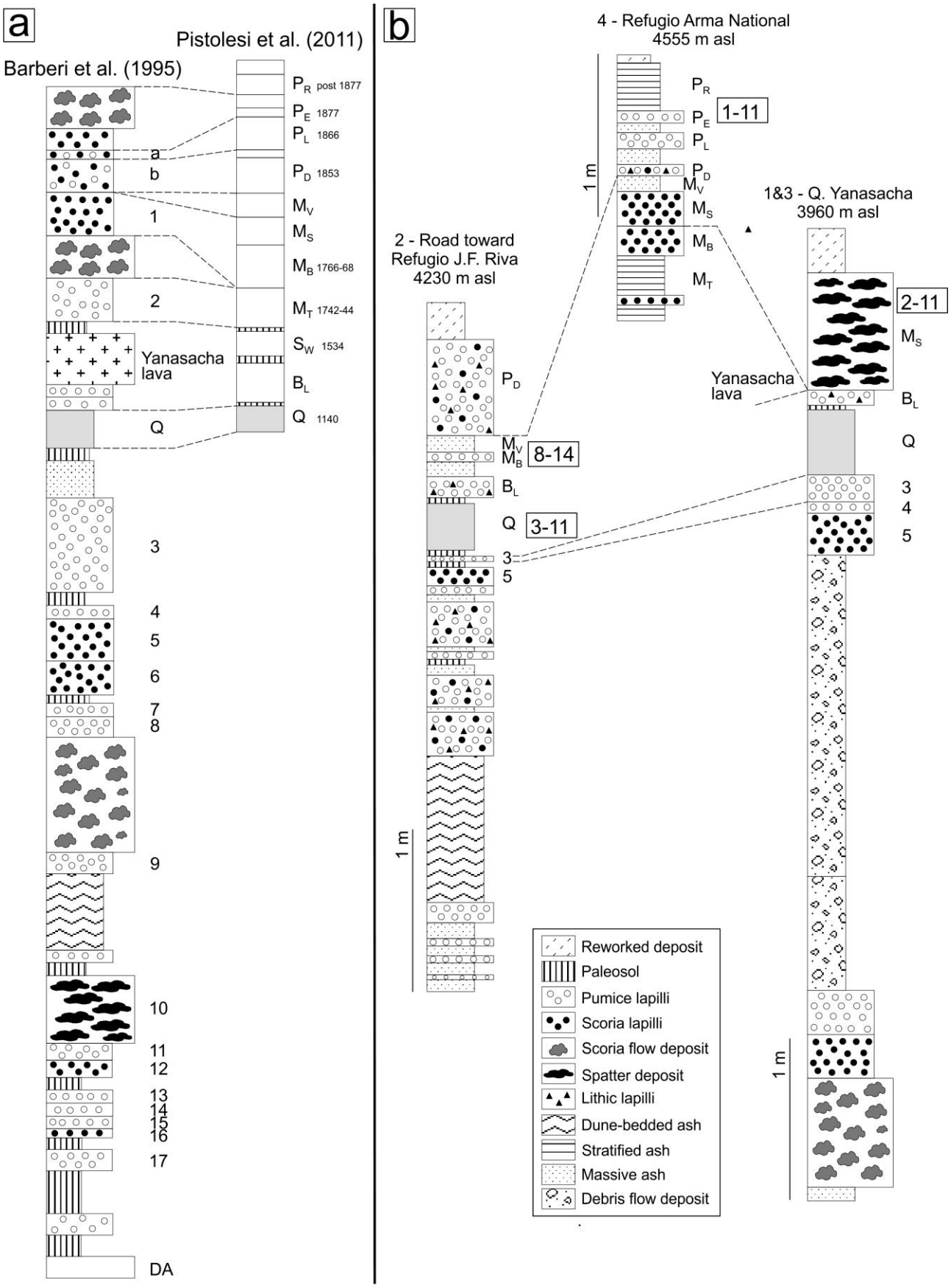

Vezzoli et al. Cotopaxi Figure 3

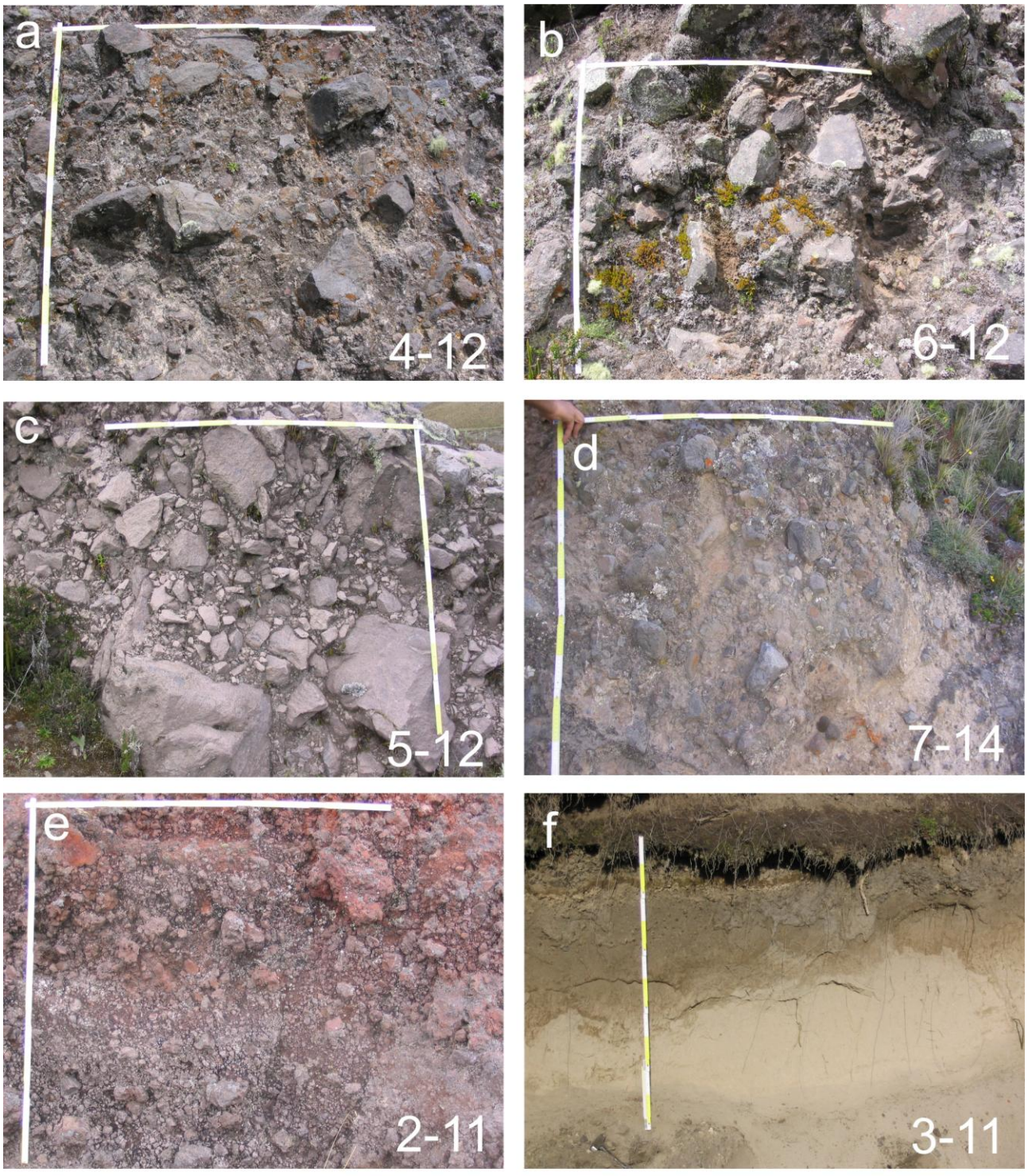

Vezzoli et al. Cotopaxi Figure 4

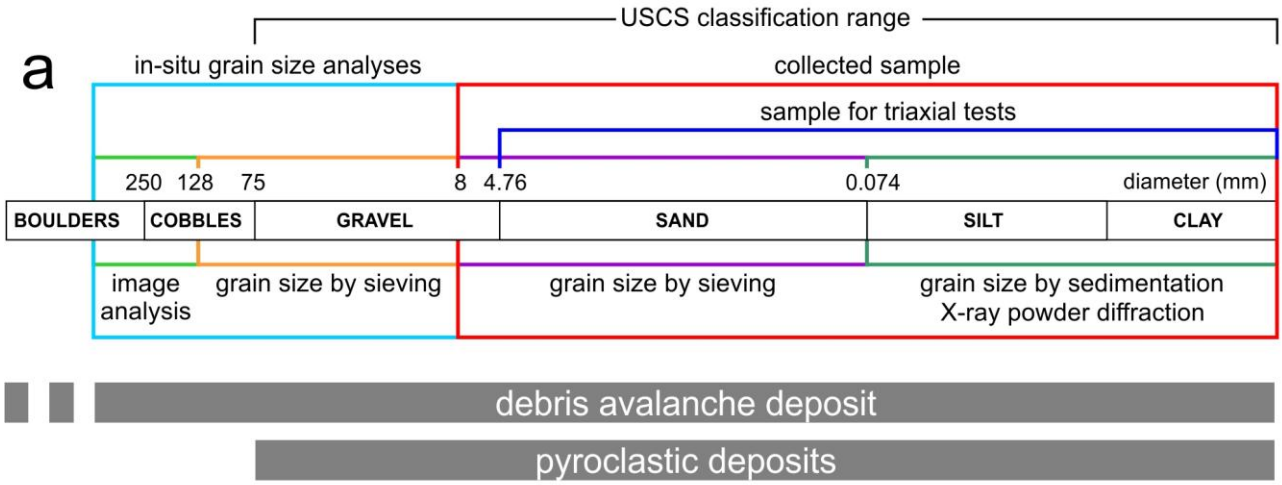

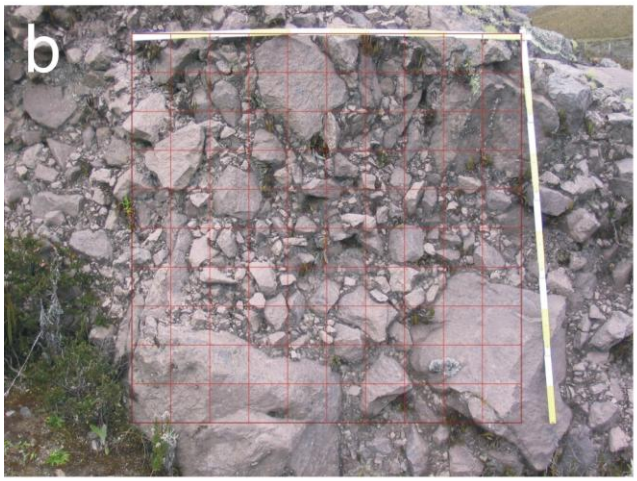

Vezzoli et al., Figure 5

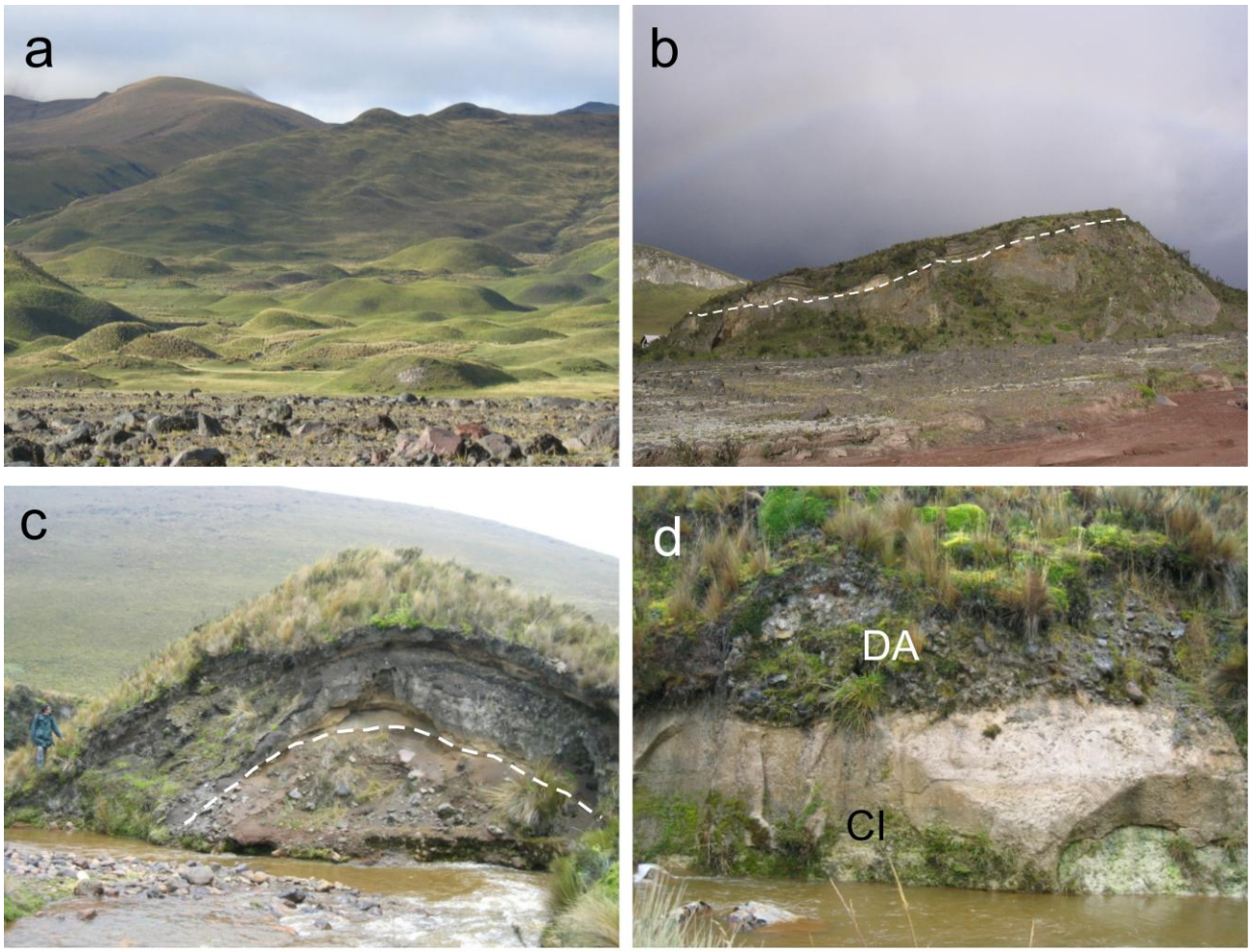

Vezzoli et al. Cotopaxi Figure 6

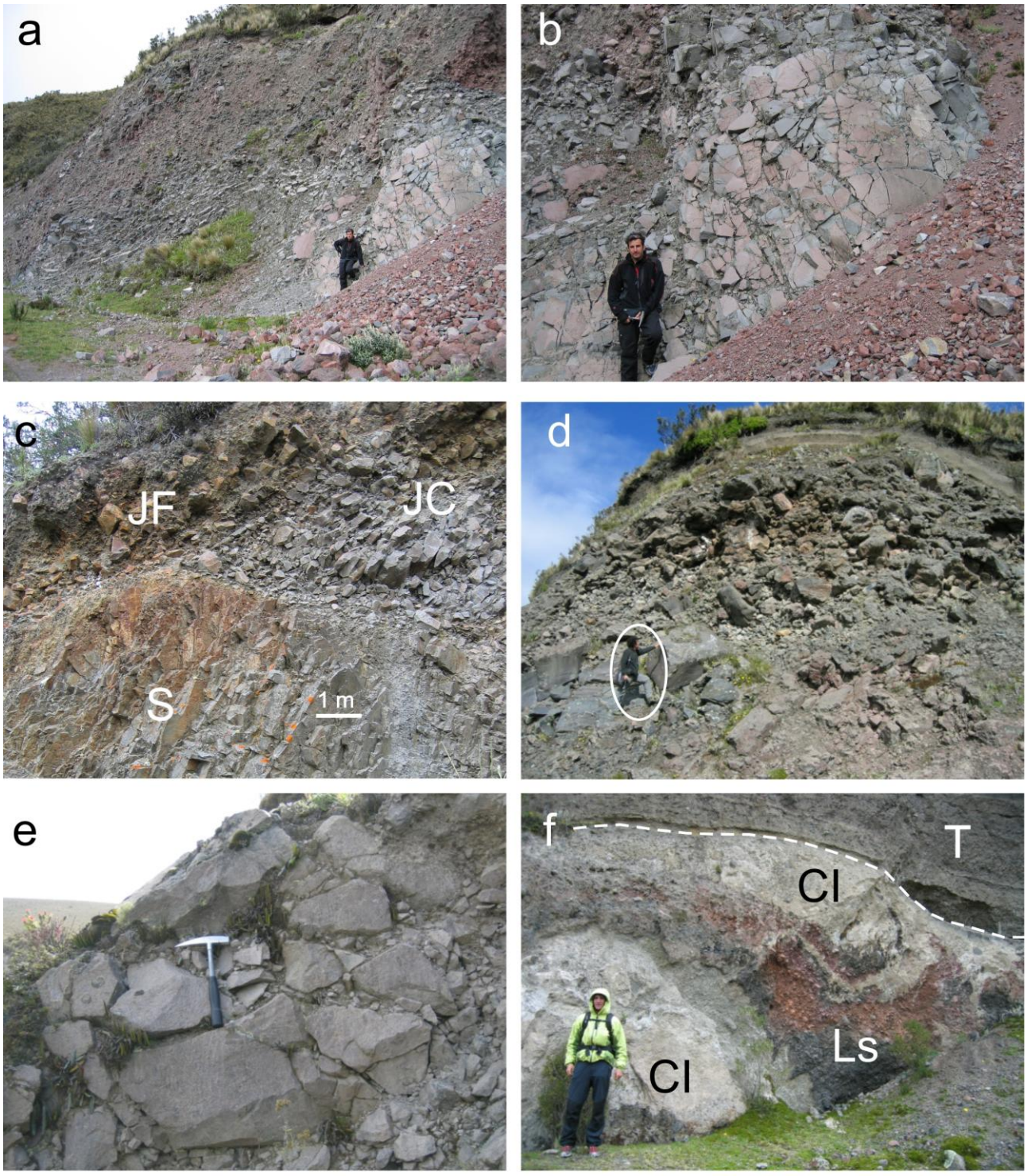

Vezzoli et al. - Cotopaxi - Fig. 7

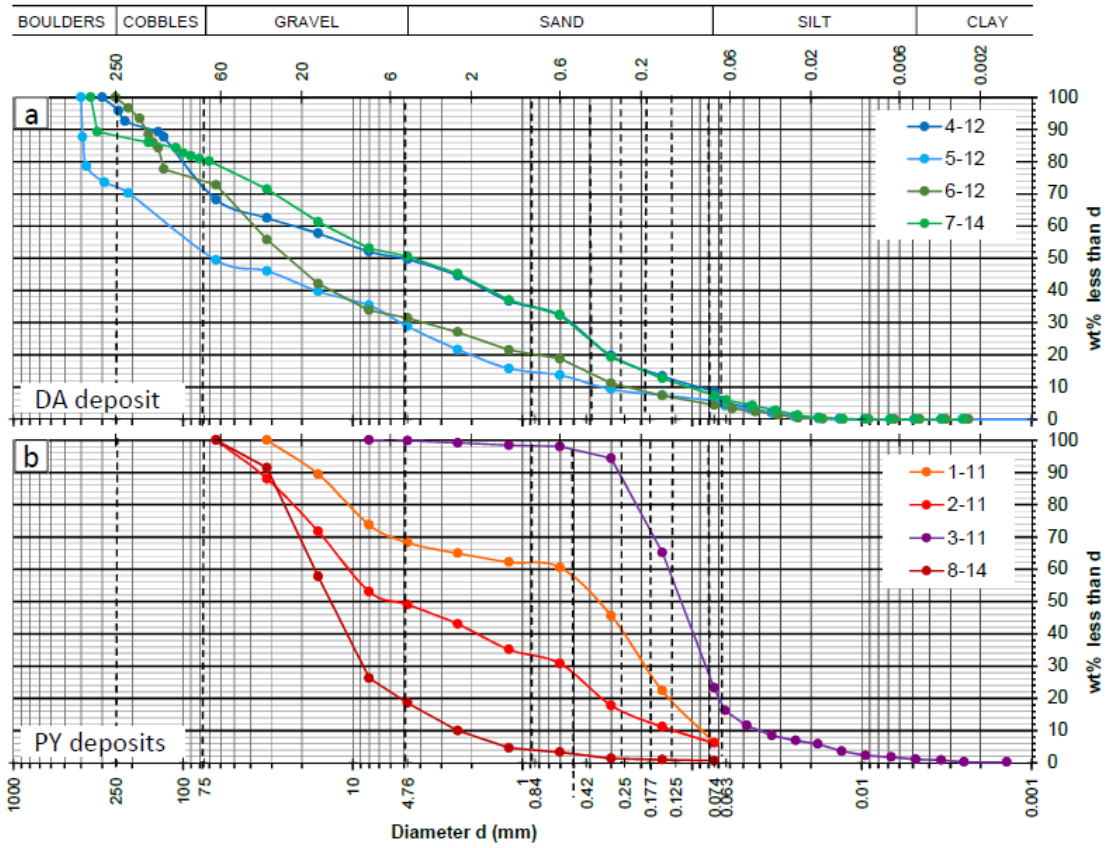

Vezzoli et al., Figure 8

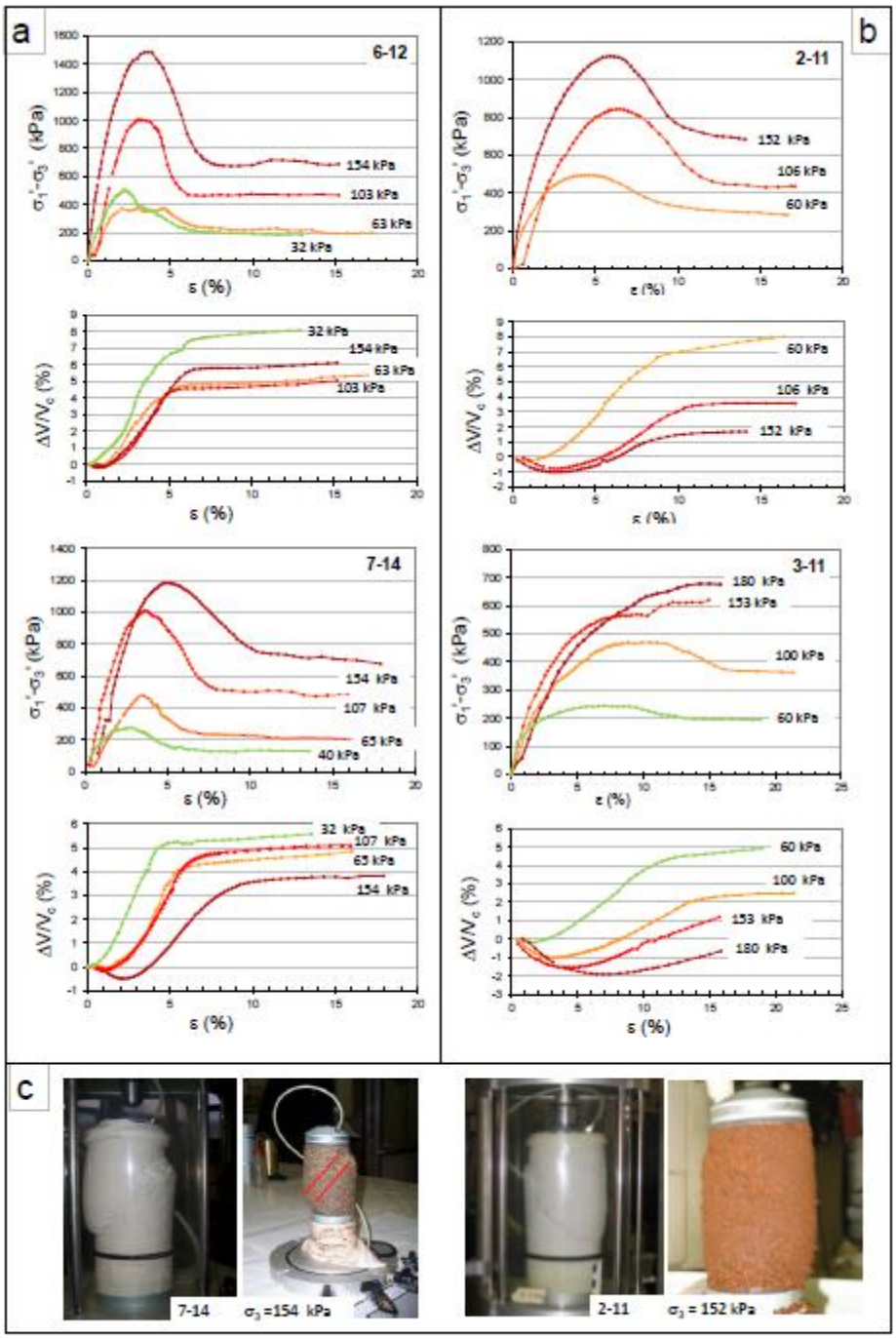

Vezzoli et al. Figure 9

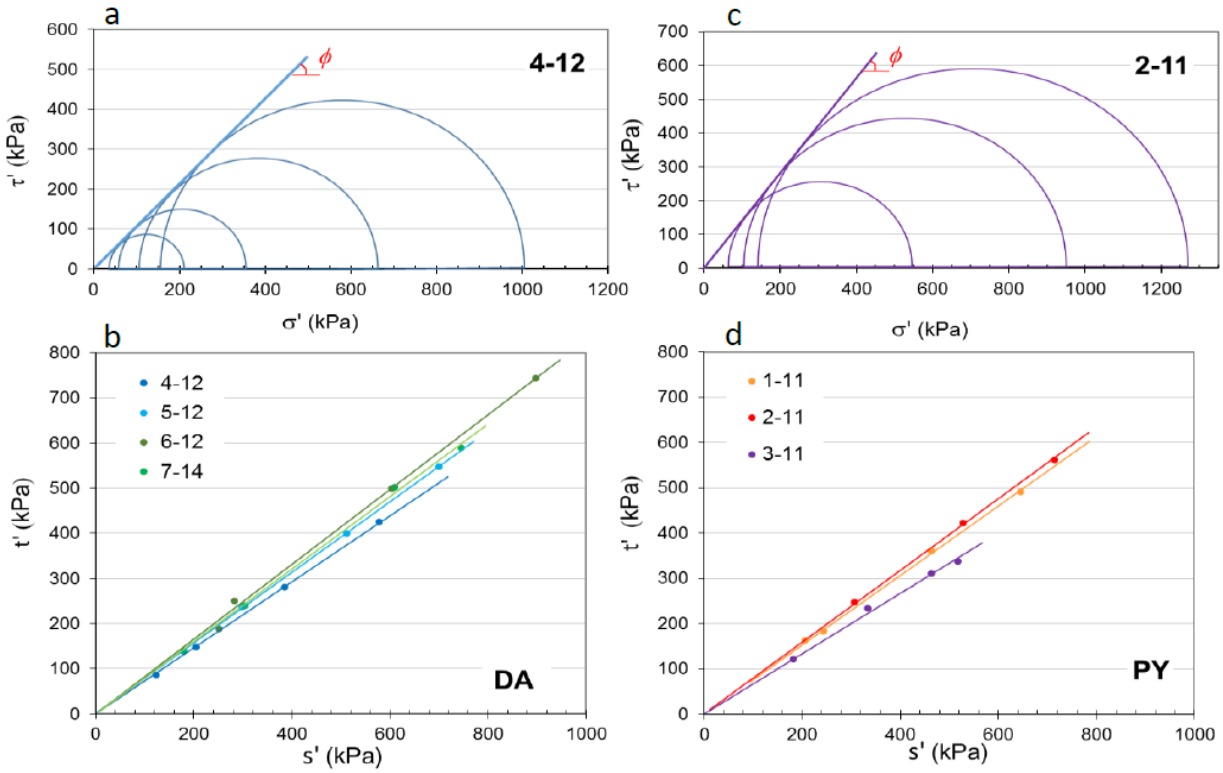

Vezzoli et al., Figure 10

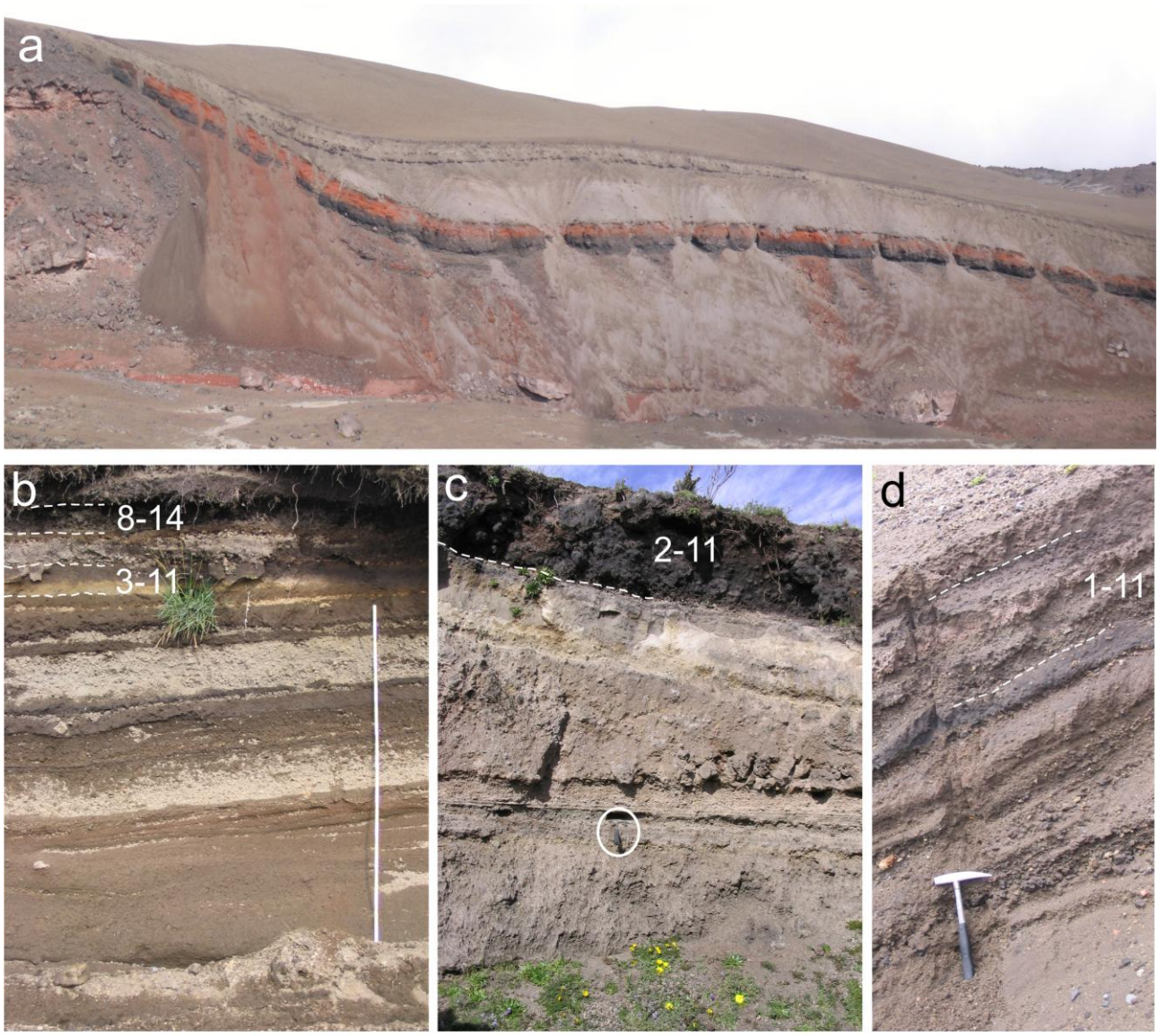

Vezzoli et al. - Cotopaxi - Fig. 11

Highlights

- Geological and geotechnical analyses of Cotopaxi's debris avalanche and pyroclastic deposits
- Correlation of DA lithofacies (megablock, block, mixed, sheared) with transport and emplacement features
- Full-range grain size characterization of debris avalanche and pyroclastic lithofacies
- Representative shear strength parameters and stress-strain behaviour determination
- Necessity for site-specific interdisciplinary approach to flank instability in volcanic successions